ANNALS OF GEOPHYSICS, 66, 6, SE645, 2023; doi: 10.4401/ag-8986
OPEN ACCESS

Lower-ionosphere anomalies prior to strong earthquakes that occurred in north-central mainland Greece on March 2021 as revealed by multi-method analysis of VLF sub-ionospheric propagation data

Dimitrios Z. Politis[1], Stelios M. Potirakis*[,1,2], Yiannis F. Contoyiannis[1], Ilyas Potamitis[3], Sudipta Sasmal[4], Shih-Sian Yang[5], Masashi Hayakawa[6,7]

(1) Department of Electrical and Electronics Engineering, Ancient Olive Grove Campus, University of West Attica, Egaleo-Athens, 12244, Greece
(2) Institute for Astronomy, Astrophysics, Space Applications and Remote Sensing, National Observatory of Athens, Metaxa and Vasileos Pavlou, Penteli-Athens, 15236, Greece
(3) Department of Music Technology & Acoustics, Hellenic Mediterranean University, Rethymnon, 74133, Greece
(4) Institute of Astronomy, Space and Earth Science, Kolkata, India
(5) Department of Space Science and Engineering, National Central University, Jhongli, Taoyuan, 320317, Taiwan
(6) Hayakawa Institute of Seismo Electromagnetics, Co., Ltd., UEC Alliance Center, #521, 1-1-1 Kojima-cho, Chofu-Tokyo, 182-0026, Japan
(7) Advanced Wireless Communication Research Center, University of Electro-Communications (UEC), 1-5-1 Chofugaoka, Chofu-Tokyo, 182-8585, Japan

Article history: received May 31, 2023; accepted August 14, 2023

Abstract

In this work we present the multi-method analysis of very low frequency (VLF) data, acquired by the radio receiver with call name UWA, located in Athens (Greece), in the University of West Attica, focusing on two strong ($M_w \geq 5.5$) earthquakes (EQs) that occurred in north-central mainland Greece sequentially, on 3 and 4 March 2021, with very close epicenters. Specifically, we used the data acquired from seven VLF transmitters located in Europe, North/North-West to UWA, and their propagation paths include the specific EQs epicenters. We analyzed these data using multiple analysis methods in order to investigate for possible EQ-related anomalies, taking also into account all the other possibly ionosphere-influencing extreme events that occurred during the studied period. Especially, we applied the "nighttime fluctuation method" (NFM), as well as, the "terminator time method" (TTM) in order to reveal any statistical anomaly in the nighttime amplitude recordings of VLF sub-ionospheric propagation data within 15 days before each one examined EQs. Also, we calculated the scalogram (wavelet power spectrum over time) using Morlet mother wavelet of the same nighttime data searching for possible imprints of wave-like structures during the same time period. In terms of criticality analysis, first we applied the "natural time" (NT) analysis method to the daily-valued NFM VLF propagation quantities, and subsequently applied the "method of critical fluctuations" (MCF) to the raw nighttime amplitude VLF recordings, to check for any criticality signatures up to two weeks before the examined EQs. Taking into account all the above-mentioned

analysis results, we conclude that there are multiple indications that the lower ionosphere was indeed disturbed due to the preparation processes of the above-mentioned EQs, offering different types of seismogenic indications.

Keywords: VLF/LF sub-ionospheric propagation data; Nighttime fluctuation method (NFM); Terminator time method (TTM); Natural time (NT) analysis; Method of critical fluctuations (MCF)

1. Introduction

Various seismo-electromagnetic (seismo-EM) phenomena have been observed before earthquakes (EQs) from the ground up to space, while an enormous effort for short-term EQ prediction has already been carried out by many scientists in the last three decades [Molchanov and Hayakawa, 1995; Pulinets and Boyarchuk, 2004; Molchanov and Hayakawa, 2008; Varotsos, 2005; Hayakawa, 2019]. For example, the subionospheric monitoring of the lower ionosphere through very low to low frequency (VLF/LF) propagation has been established as a wide-spread radio-technique for searching electromagnetic (EM) signatures in the signal (amplitude and phase) characteristics which are associated with many different extreme events such as EQs, volcanoes, geomagnetic storms, solar flares and typhoons, [e.g., Malkotsis et al., 2022; Rozhnoi et al., 2014a, 2014b; Hayakawa, 2011; Nina et al., 2021].

On the other hand, multiparametric studies have yielded important findings strengthening the assumption of the lithosphere-atmosphere-ionosphere coupling (LAIC) mechanism, which is key in understanding the possible cause(s) and their effect to each parameter [Piersanti et al., 2020; Sasmal et al., 2021; Hayakawa et al., 2021, 2022]. The involved parameters have extensively been used together or separately to investigate the possible correlation between the time of the occurrence of the EQ and the time of appearance of the anomaly. These parameters are grouped into five supposed characteristic channels (electromagnetic, electrostatic, thermal, acoustic and chemical) of the LAIC, where some of them can be found to be interconnected in a way that the one can possibly trigger the other [Hayakawa, 2019; Pulinets & Ouzounov, 2011; Pulinets et al., 2022]. In this perspective, several scientific works have recently been published in the literature including a vast variety of EQ-related anomalies, [e.g., Ghosh et al., 2021, 2023; Chakraborty et al., 2018; Conti et al., 2021; Picozza et al., 2021].

Another important direction in the field of possible seismic precursors is the application of criticality analysis to various parameters of the LAIC model. Such studies have revealed that different layers of the model reach critical state before a strong EQ occurrence. Specifically, the criticality analysis method called "natural time" (NT) analysis has successfully been applied to VLF subionospheric propagation data, ULF magnetic field data, global navigation satellite system deformation (GNSS) data, surface latent heat flux (SLHF) data and very recently in stratospheric potential energy (E_p), as well to other EQ-related observables such as pre-EQ seismic electric signals (SES), foreshock seismicity, MHz fracto-EM Emissions, also known as fracto-EM Radiation, (FEME/FEMR), [e.g., Politis et al., 2021, 2022; Potirakis et al., 2013, 2018a, 2021; Yang et al., 2020; Ghosh et al., 2021; Varotsos et al., 2011, Eftaxias et al., 2018]. Additionally, another criticality analysis method called "method of critical fluctuations" (MCF) has been also applied in VLF subionospheric propagation data, MHz FEME/FEMR recordings and ULF magnetic field data [Politis et al., 2021; Potirakis et al., 2016, 2018b, 2019; Contoyiannis et al., 2004a].

In this work we used the VLF subionospheric propagation data taken from a VLF/LF receiver which has been installed in the beginning of 2020 at the Department of Electrical and Electronics Engineering of the University of West Attica (with call name UWA) (geographic coordinates: 37.977° N, 23.673° E) in Athens (Greece). More, specifically, we analyzed the VLF data of the UWA station received from seven VLF transmitters, which are located in Europe. Specifically, in this investigation, we examined two strong EQs, that occurred very close in time and had very close epicenters. These had magnitudes of 6.3 M_w and 5.8 M_w and occurred on 3 and 4 March 2021, respectively, at the region of Thessaly in north-central mainland Greece (please see more information in Section 2). Henceforth, when we refer to both them, we call them "the 2021 Thessaly EQs", the 3 March 2021 one will be referred to as the "1st 2021 Thessaly EQ", while the 4 March 2021 one as the "2nd 2021 Thessaly EQs".

In the present study, we used the same statistical and criticality analysis methods that have already been used for 2020 Samos EQ, which occurred in Greece on 30 October 2020 [Politis et al., 2021]. The statistical methods

are the nighttime fluctuation method (NFM) and terminator time method (TTM), which have widely been used, especially in Japan, searching for EQ-related anomalies in the characteristics of VLF subionospheric propagation data [Hayakawa, 2007, 2011; Hayakawa et al., 1996a, 1996b]. On the other hand, the herein employed criticality analysis methods (NT and MCF) have also been applied to VLF subionospheric propagation data, e.g., prior to the 2016 Kumamoto EQs in Japan, proving the existence of criticality in the lower ionosphere [Potirakis et al., 2018a, 2018b]. Beyond the analysis of VLF nighttime amplitude data using the aforementioned methods, we also calculated the scalogram (wavelet power spectrum over time) using Morlet mother wavelet. This analysis method has been applied, for example, in the VLF nighttime amplitude recordings before the 2016 Imphal EQ searching for possible existence of atmospheric gravity waves (AGWs) in the form of wave-like structures, two weeks before the impending mainshock [Biswas et al., 2020]. More specifically, we analyzed the raw amplitude recordings using the statistical analysis methods (NFM and TTM), while we applied the NT analysis method to the three daily-valued NFM VLF propagation quantities. In addition to the analysis of these data we also applied the "Morlet wavelet analysis" in order to search for any possible embedded signature of atmospheric gravity waves (AGWs) by taking the same nighttime interval as in the case of application of NFM. Finally, as a second step in criticality analysis, we applied the MCF method to the raw nighttime amplitude recordings, to check for any criticality signatures before the occurrence of each of the studied EQs.

The results obtained from the application of all the above-mentioned analysis methods to the VLF amplitude data received from seven transmitters by a VLF/LF receiver located in Athens, Greece, show significant pre-seismic signatures in the lower ionosphere within 15 days before the 2021 Thessaly EQs. Moreover, some other possibly ionosphere-influencing geophysical and space extreme events, which occurred in close time with the examined EQs, were also carefully taken into account.

The rest of this paper is organized as follows: In Section 2 we provide the information about the studied EQs, the subionospheric propagation data used, as well as any other possibly ionosphere-influencing geophysical and space extreme events that occurred during the studied period. In Section 3 we briefly present the employed time series analysis methods, while in Section 4 we present the analysis results. Finally, Section 5 summarizes the conclusions.

2. Sub-Ionospheric propagation data, studied EQs and other possibly ionosphere-influencing extreme events

As already mentioned in Section 1, in this article we investigate two relatively strong EQs ($M_w \geq 5.5$ which occurred in north-central mainland Greece on 3 and 4 March of 2021 and their epicenters were located, very close to each other, in a land area within the municipality of Tyrnavos in the prefecture of Larissa in Thessaly region. Table 1 provides detailed information (acquired from the seismic catalog of the United States Geological Survey (https://earthquake.usgs.gov/ (accessed on 19 May 2023)) about the EQs of interest. It is noted that the lower ionosphere, among other geophysical and space extreme events, is sensitive to EQs, so it is expected that the 2021 Thessaly EQs, having $M_w \geq 5.5$, could probably have affected the ionosphere, [e.g., Rozhnoi et al., 2013].

In this study we chose to use data from seven transmitters that are continuously recorded by the VLF/LF receiver with call name "UWA", which is installed in the Electronics & Computer Technologies Lab (ECTLab) (http://ectlab.eee.uniwa.gr/index.php/en/ (accessed on 19 May 2023)), belonging to the Department of Electrical and Electronics Engineering of the University of West Attica in Athens (Greece) (37.977° N, 23.673° E). A detail description of the

Order of occurrence	Date	Time (UT)	M_w	Depth (km)	Latitude	Longitude
1st	3 March 2021	10:16:09	6.3	8.0	39.755° N	22.176° E
2nd	4 March 2021	18:38:19	5.8	10.0	39.787° N	22.116° E

Table 1. Information about the 2021 Thessaly EQs as provided by the United States of Geological Survey (USGS) (https://earthquake.usgs.gov/ (accessed on 19 May 2023)). "UT" stands for universal time.

Call name	Country	Operating frequency (kHz)	Latitude	Longitude	Distance from UWA (km)
JXN	Norway	16.400	66.9827° N	13.8731° E	3280
GBZ	UK	19.580	54.9112° N	3.2813° W	2760
ICV	Italy	20.270	40.9231° N	9.7310° E	1240
FTA	France	20.900	48.5401° N	2.5502° E	2060
HWU	France	21.750	46.7130° N	1.2444° E	2070
DHO	Germany	23.400	53.0819° N	7.6163° E	2100
NRK	Iceland	37.500	63.8503° N	22.4664° W	4160

Table 1. Information about the VLF transmitters monitored by the UWA receiver, which were used in this study.

hardware and software of the specific VLF/LF observation station and the transmitters monitored is provided in Politis et al. [2021], while the sampling frequency of the recordings is 1 Hz. It is noted that in this study we used the raw amplitude recordings taken from daily files, in txt format, and specifically only their nighttime parts (see also Section 3). Table 2 summarizes key information about the transmitters used in this work (call name, country, operating frequency, location coordinates, and great circle path distance from the UWA receiver). Figure 1 presents

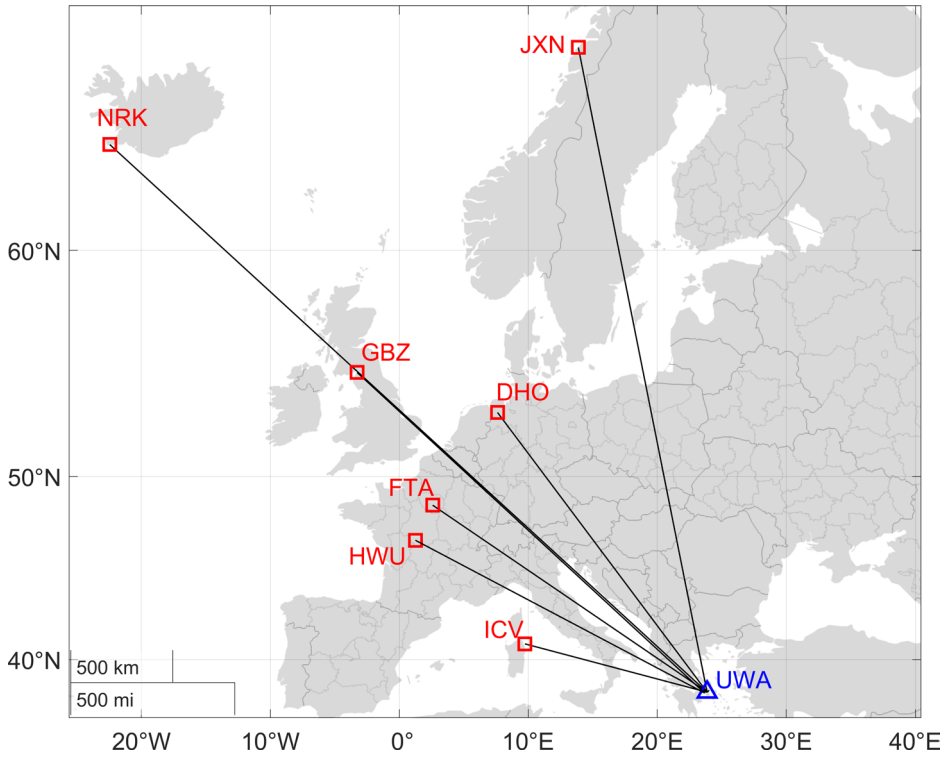

Figure 1. Map of the wider area of Europe (and some part of western Asia). The locations of the seven transmitters which were used in this study are marked by red squares, whereas the location of the receiver is shown as a blue triangle. The black lines represent the shortest path links between each transmitter and the receiver.

a map on which the locations of the considered transmitters and the receiver are marked, along with their call names and the shortest path links between each transmitter and the receiver. Moreover, Fig. 2 depicts the fifth Fresnel zones of the considered VLF subionopsheric propagation paths on the same map with the epicenters of the examined EQs (focusing on the geographic area of the EQs of interest). As evident from Fig. 2, the 2021 Thessaly EQs occurred within the fifth Fresnel zones of all the considered propagation paths, except for the case of the ICV-UWA path for which the specific EQs epicenters were really close to the borders of the corresponding fifth Fresnel zone.

In this study we also checked for any other possibly ionosphere-influencing geophysical and space extreme events, such as geomagnetic storms, solar flares, thunderstorms, typhoons, volcanos, or significant ($M_w \geq 5.5$) EQs other than the EQs of interest, which occurred in close time with the investigated EQs, specifically within a period of two months starting from 1 February 2021 to 31 March 2021, and could possibly affect our analysis results (see Section 4).

First, we checked the United States Geological Survey (USGS) seismic catalog for any significant ($M_w \geq 5.5$) EQs, with epicenters within (or close to) the considered fifth Fresnel zones, taking into account the whole geographic area of these paths (see Fig. 1). We have found four such cases. The first EQ was of magnitude 5.5 M_w and occurred on 17 February 2021 03:36:07 (UT), in Phocis, Greece (38.406°N, 22.019°E), with focal depth 5.3 km. The second EQ's magnitude was 5.6 M_w and occurred on 24 February 2021 10:05:59 (UT), 6 km southeast of Vogar town in Iceland (63.949 °N 22.285 °W), with focal depth 10 km, which likely only affects the NRK-UWA sub-ionospheric propagation path. The third EQ was a 5.6 M_w aftershock of the 2021 Thessaly EQs that occurred on 12 March 2021 12:57:50 (UT), 8 km west of Elassona town (39.893 °N 22.088 °E), with focal depth 7 km. The last one was a 5.5 M_w EQ that occurred on 27 March 2021 13:47:55 (UT) in the Adriatic Sea (42.448°N, 16.050°E), with focal depth 7 km, 55 km north of Peschici (Foggia) in Italy. All these EQs except from the one having epicenter at Vogar town in Iceland (which is too far from the area of interest) are depicted in Figure 2.

Furthermore, we checked for any geomagnetic storms or solar flares. Although, as already mentioned, we used only nighttime data in our analyses, it is noted that no solar flares of the M or X class were observed during the studied period according to the X-ray flux index from the National Oceanic and Atmospheric Administration (NOAA) (https://www.swpc.noaa.gov/products/goes-x-ray-flux (accessed on 19 May 2023)). Figure 3 portrays the variation

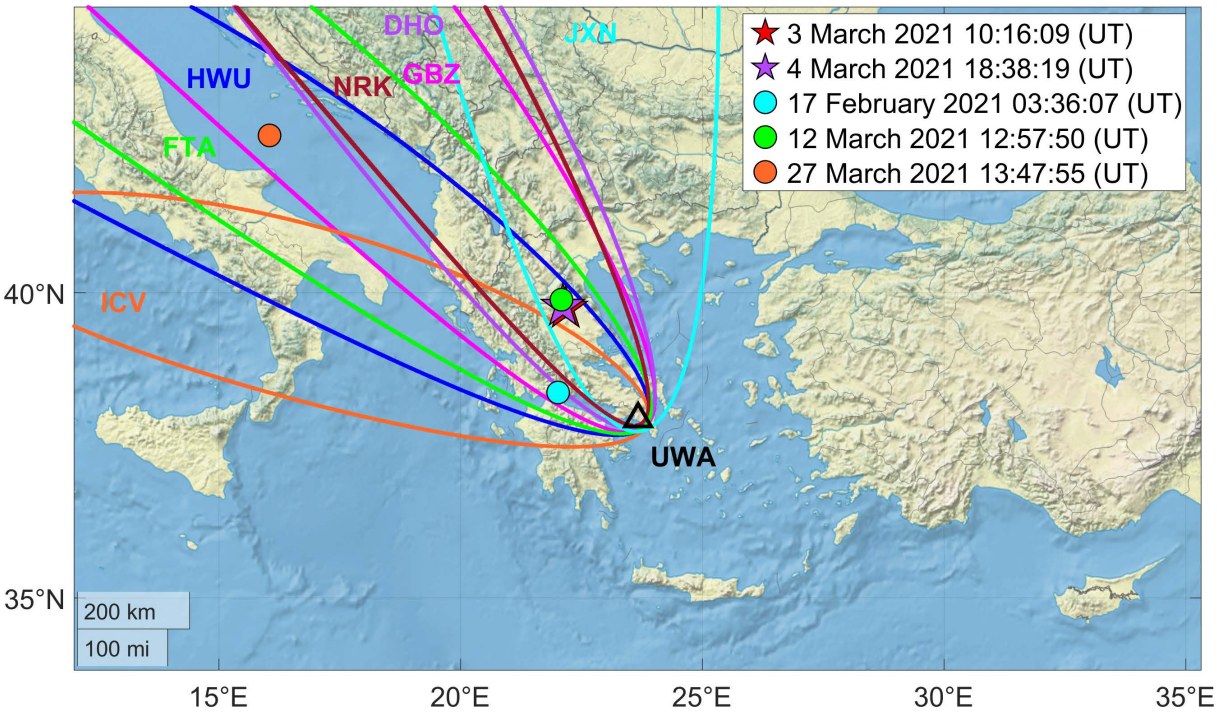

Figure 2. Map showing a part of the area of east Mediterranean including Greece and neighboring countries. The parts of the studied paths' fifth Fresnel zones falling within the specific geographic area are shown with different colors, while the call names of the corresponding transmitters are also indicated and accordingly colored. The stars represent the epicenters of the studied 2021 Thessaly EQs, while three other EQs that occurred in the depicted area during the examined time period are also shown as circles.

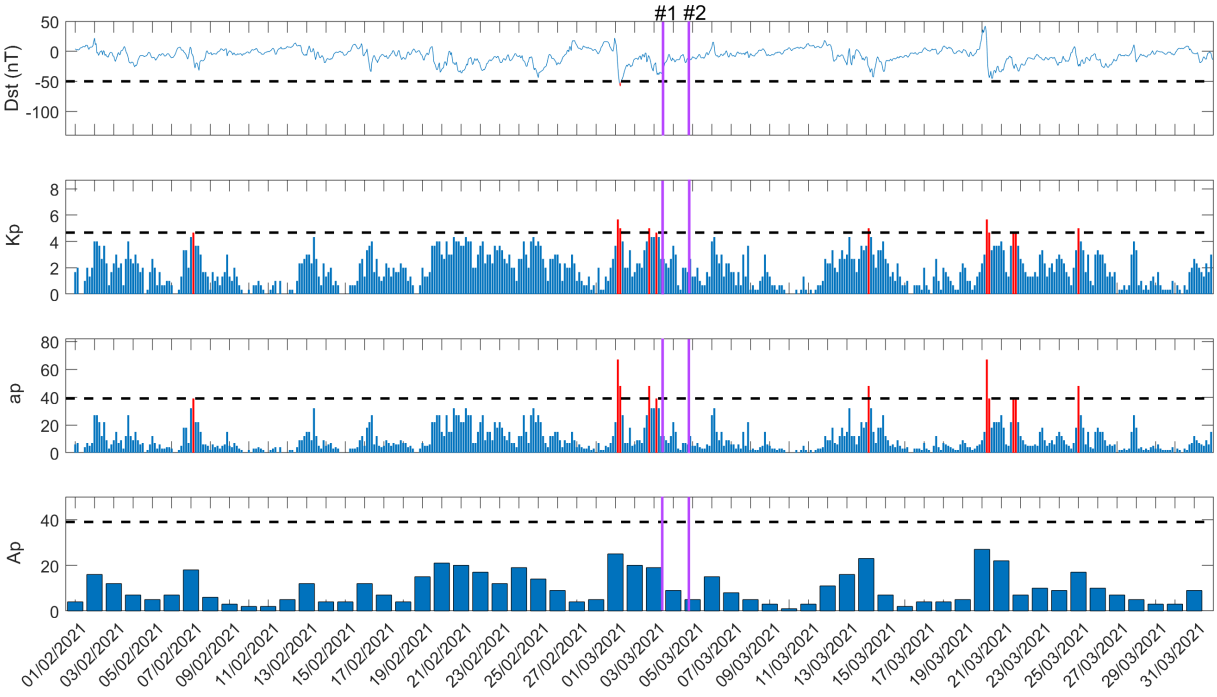

Figure 3. Temporal variation of geomagnetic indices during the time period 1 February 2021 – 31 March 2021 (from top to bottom panel): Dst, Kp, ap, and Ap. Red colored parts indicate values exceeding the corresponding thresholds marked by the horizontal black dashed lines. The solid vertical purple lines in each panel indicate time of occurrence (see Table 1) of the two studied 2021 Thessaly EQs.

of the 1-hour (sampling period) Dst index, the 3-hour Kp index, the 3-hour ap index, as well as, the daily variation of Ap index in four panels, covering the time period from 1 February 2021 to 31 March 2021. The Dst, Kp, ap and Ap data were acquired from the world data center (WDC) for geomagnetism of Kyoto (https://wdc.kugi.kyoto-u.ac.jp/wdc/Sec3.html (accessed on 19 May 2023)). As we it can be seen from Fig. 3, a minor geomagnetic storm of $(\mathrm{Dst})_{\mathrm{min}} = -58$ nT was recorded on 1 March 2021 (06:00 UT), with simultaneous significant enhancements of Kp and ap indices. Very small sporadic excesses of Kp index occurred on 2, 3, 14, 20, 21 and 25 March of 2021, simultaneously with increases in the ap index. However, these indications are not accompanied with significant (< -50 nT) decreases of the Dst index.

Moreover, after checking the convective available potential energy (commonly abbreviated as CAPE), as an indication of atmospheric instability, using the Ventusky search engine (https://www.ventusky.com (accessed on 19 May 2023)) we found that no thunderstorms were recorded during the investigated time period (1 February 2021 to 31 March 2021). At this point, it should be mentioned that we have also checked the lighting activity from "Blitzortung.org" lightning detection network (https://www.blitzortung.org/en/historical_maps.php (accessed on 19 May 2023)) and "lightningmaps.org" (https://www.lightningmaps.org/ (accessed on 19 May 2023)), and no lightning activity was recorded during the specific time period. Finally, according to the Global Volcanism Program of the Smithsonian Institution (https://volcano.si.edu/search_eruption.cfm (accessed on 19 May 2023)), there was one confirmed eruption (unknown VEI) of Fagradalsfjall volcano in Iceland, which occurred on 19 March 2021, which could affect only the NRK-UWA sub-ionospheric propagation path (see Fig. 1).

3. Analysis Methods

This section, briefly provides key information about the analysis methods that were used in the present article. Specifically, in Section 3.1 we briefly present the NFM statistical method, while in Section 3.2 we present the TTM statistical method using the concept of terminator time (TT) shifts. Section 3.3, provides information about the wavelet analysis employed. Finally, we present the criticality analysis methods NT analysis and MCF in Sections 3.4 and 3.5, respectively.

3.1 Nighttime fluctuation method (NFM)

The nighttime fluctuation method (NFM) was proposed for the detection of anomalies (increases or decreases) caused by ionospheric disturbances in relation with a variety of ionosphere-influencing extreme events such as EQs [Malkotsis et al., 2022; Hayakawa, 2011]. First of all, the raw nighttime amplitude data (in dB) are extracted from the diurnal variation of the amplitude data, by appropriately selecting a nighttime interval of adequate length of samples (the station records at a sampling frequency of 1 Hz), in order to exclude working (daytime) hours during which anthropogenic noise may be present. Terminator times which are represented as minima in the amplitude of the signal (and a sufficient margin from them) are not included to the nighttime interval, since ionosphere-influencing extreme events may result to shift of terminator times, which is analyzed separately (see Section 3.2). After the determination of the appropriate nighttime interval, the next step is to calculate the mean of value (denoted as $\langle A(t) \rangle$) of $\pm$ 15 days around the day of interest, plus the day of interest. Subsequently, the residual variation of the amplitude of the signal, defined as $dA(t) = A(t) - \langle A(t) \rangle$, is calculated, where $A(t)$ is the signal of the amplitude at the time t. The usage of $\pm$ 15 days sliding window reduces the "long-term" variations to unveil the "short-term" variations. Finally, the daily values for the three statistical parameters "TR" (trend), "DP" (dispersion) and "NF" (nighttime fluctuation) are calculated, as:

$$TR = \frac{\sum_{N_s}^{N_e} dA(t)}{N_e - N_s}, \tag{1}$$

where TR represents the mean value of $dA(t)$, and N_e and N_s are the start and end points of the chosen nighttime interval (starting and ending time points),

$$DP = \sqrt{\frac{1}{N_e - N_s} \sum_{N_s}^{N_e} (dA(t) - TR)^2}, \tag{2}$$

where the DP is actually the standard deviation of $dA(t)$, and

$$NF = \sum_{N_s}^{N_e} \left(dA(t) \right)^2. \tag{3}$$

After the calculation of the daily valued time series of the above mentioned three statistical quantities we compute their normalized values TR^*, DP^*, and NF^* as $X^* = (X - \langle X \rangle_{\pm 15})/\sigma_{\pm 15}$, where $\langle X \rangle_{\pm 15}$ and $\sigma_{\pm 15}$ are the mean value and the standard deviation of $\pm$ 15 days around the day of interest, respectively. Any statistical anomaly in these daily valued time series that exceeds $\pm 2\sigma$ could possibly be related to an EQ's preparation process or any other possibly ionosphere-influencing extreme event that can affect nighttime data [Politis et al., 2021; Hayakawa, 2011; Tatsuta et al., 2015; Malkotsis et al., 2022]. In fact, this method has recently been applied extensively to identify ionospheric anomalies prior to EQs as an increase in TR and decrease in DP and NF, [e.g., Rozhnoi et al., 2004; Politis et al., 2021; Hayakawa, 2011]. It should be mentioned that generally the usage of a $\pm$ 15 days window around the day of interest includes information from the "future", so this is appropriate only for à posteriori analysis [Politis et al., 2021]. To do analysis in "real time" one should use a single-sided window.

3.2 Terminator time method (TTM)

The terminator time method (TTM) was proposed for the statistical analysis of the occurrence time of the minima in the amplitude or/and the phase of the VLF signal [Hayakawa, 2007, 2011; Hayakawa et al., 1996a, 1996b] which are close in time to the local (planetary) sunrise time and sunset time. These minima are referred to as sunrise terminators (SRTs) and sunset terminators (SSTs), respectively, or generally as terminator times (TTs), and are

created from the interference of different propagation waves (modes of propagation) of the VLF signal, that is, the ground wave and the sky wave [Hayakawa et al., 1996a, 1996b].

A significant shift in the SRTs or SSTs, as compared with neighboring days, is considered to be an anomaly induced by an EQ, when the lower ionospheric height is normally decreased [Yoshida et al., 2008]. In other words, an earlier appearance of an SRT or a later appearance of an SST, which means an anomalous increase of the duration of the "VLF-day" ("VLF-daylength", D_{VLF}) as compared with the previous days, is considered to be an EQ precursor [Hayakawa et al., 1996a, 1996b].

The TTM was initially applied to the strong Kobe EQ (M7.1) that occurred in Japan on 17 January 1995, before which significant shifts in the TTs were found [Hayakawa et al., 1996a, 1996b; Molchanov et al., 1998]. By this concept several other studies have also reported shifts in TTs, and consequent increases in D_{VLF}, before an impending EQ [Ray et al., 2013; Sasmal & Chakrabarti, 2009; Sasmal et al., 2010; Chakraborty et al., 2017]. Many other statistical studies have also reported correlations between EQs and TT anomalies, with maximal shifts occurring 0-4 days prior to the EQ [Chakrabarti et al., 2005, 2007, 2010; Ray et al., 2010, 2011, 2012, 2013; Sasmal et al., 2014; Pal et al., 2017]. Furthermore, some studies based on numerical simulation of the diurnal variation of the amplitude of the VLF signal, taking into consideration the characteristics of the VLF propagation path, the transmitter, and the receiver, have been applied for the determination of TTs [Chakraborty et al., 2017; Ghosh et al., 2019; Biswas et al., 2022].

In applying the TTM, one has to initially locate the time of appearance of two minima in the diurnal variation of the signal (amplitude or phase), which are close in time with the planetary sunrise and sunset time of each day, respectively. Using these time locations, which are the morning and evening TTs, two TT time series are formed, one for the morning minima, denoted as t_m, and one for the evening minima, denoted as t_e. Subsequently, using a time window of $\pm$ 2 days around the day of interest window (including the day of interest), i.e., of 5 days width, the running mean for each of the aforementioned time series is calculated, forming two new time series designated as t_m and t_e, for the morning and evening TTs, respectively. Finally, the running mean time series are subtracted from the respective TT time series to form the residual TT time series $dt_m = t_m - \langle t_m \rangle$ and $dt_e = t_e - \langle t_e \rangle$, respectively [Hayakawa et al., 1996a, 1996b; Molchanov et al., 1998]. Moreover, the VLF-daylength is calculated as $D_{VLF} = t_e - t_m$, and similarly to the TT time series, the running mean time series D_{VLF} and the residual VLF-daylength time series $dD_{VLF} = D_{VLF} - \langle D_{VLF} \rangle$ are subsequently calculated. Any statistical anomaly in the residual TTs or the residual VLF-daylength, exceeding $\pm 2\sigma$ of the whole considered time period, is investigated as possibly being EQ-related.

3.3 Wavelet analysis

Wavelet analysis here refers to the calculation of the time-scale representation of signal's power called scalogram [Torrence and Compo, 1998], which in the case of VLF nighttime amplitude recordings is performed by applying the continuous wavelet transform to overlapping segments (time windows) of an appropriately preprocessed version of the raw VLF signal, as explained in the following, providing thus a temporal evolution of its wavelet power spectrum (WPS). It is noted that the wavelet transform is a kind of multi-resolution analysis (analysis of the signal at different scales with different resolutions; specifically, large scale corresponds to "overall view", or long-term behavior, while small scale corresponds to "detail view", or local behavior) and is defined as the convolution of the signal under analysis with a set of wavelet functions generated by the "mother wavelet" by dilation and translation [Daubechies, 1992; Mallat, 1998; Stark, 2005; Contoyiannis et al., 2013]. Note that scale could be considered corresponding to the inverse to "frequency", i.e., "period", if one likes to refer to Fourier analysis terms. Scalogram presents the different scale components of the signal over time, unveiling thus periodicities of "wave-like" structures of the signal [Torrence and Compo, 1998].

For example, in VLF nighttime amplitude recordings, periodicities have been revealed in a period from 1 to 128 minutes prior to the Imphal EQ which occurred in India on 4 January of 2016 ($M = 6.7$) [Biswas et al., 2020]. These "wave-like structures" are associated with the existence of the preseimic AGWs emitted around the epicenter of EQ, which directly affect the lower ionosphere and consequently the nighttime amplitude recordings of the signal [Biswas et al., 2020].

The calculation of VLF nighttime amplitude recordings' scalogram is performed according to the following procedure. First, the original data are resampled from 1 s to 1 min. Then from each 1 min sampled amplitude value its ten-minute running mean is subtracted, resulting to the residual amplitude of the VLF signal. Subsequently, the scalogram is computed using the Morlet mother wavelet function, by applying the continuous wavelet transform

to fixed length overlapping time windows of the above-mentioned preprocessed version of the original VLF signal (namely, to the residual amplitude). Finally, the cone of influence (CoI) is overplotted on the scalogram, representing the boundary beyond which the scalogram values are not reliable, due to the addition of zeros (zero padding), which is required to convert the total number of data points to a power of two to compute the scalogram [Torrence and Compo, 1998; Biswas et al., 2020].

3.4 Natural time method

The NT time series analysis method has initially been applied to the ultra-low frequency (≤ 1 Hz) seismic electric signals (SES) [Varotsos et al., 2001, 2002, 2005], and has been shown to be optimal for enhancing the signals in the time-frequency space [Abe et al., 2005]. The full theoretical details of this method can be found in the book of Varotsos et al. [2011] (and references therein), while the application of NT analysis to various seismo-EM signals, including VLF sub-ionospheric propagation data has been presented in detail in [Potirakis et al., 2021]. Also, newer studies using the NT time series method to other observable quantities of LAIC have shown existence of critical dynamics before EQs [Ghosh et al., 2021; Yang et al., 2020; Politis et al., 2022]. Furthermore, a very recent application of NT time series method to global seismicity is given by Christopoulos et al. [2022]. In the following, we briefly present the key notions of this method and the process of applying it to VLF sub-ionospheric propagation data.

Initially, for a number of N events, we determine the NT of the k-th (in order of occurrence) event as:

$$\chi_k = k/N, \tag{4}$$

which is actually the order of occurrence normalized in the interval (0,1]. Next, we determine the "energy" of each event in NT, which is denoted as Q_k for the k-th event. At this point we have to mention that Q_k corresponds to different kinds of quantities, depending on the time series under analysis. For example, in the case of seismic events Q_k is the seismic energy released (seismic moment), while for the dichotomous SES signals Q_k corresponds to the SES pulse duration [Varotsos et al., 2005]. On the other hand, in the case of the FEME/FEMR signals in the MHz band, which are non-dichotomous signals, Q_k denotes the energy of each event calculated using consecutive amplitude values above a noise threshold as described in [Potirakis et al., 2013].

Then, we study the resulting time series (χ_k, Q_k). The approach of a dynamical system to criticality is identified by means of the variance $\kappa_1 = \langle \chi^2 \rangle - \langle \chi \rangle^2$ of NT, where $\langle f(\chi) \rangle = \sum_{k=1}^{N} p_k f(\chi_k)$ and $p_k = {Q_k}/{\sum_{n=1}^{N} Q_n}$ is the normalized energy released during the k-th event. Hence, the quantity κ_1 can be written as:

$$\kappa_1 = \sum_{k=1}^{N} p_k \chi_k^2 - \left(\sum_{k=1}^{N} p_k \chi_k \right)^2. \tag{5}$$

Moreover, the entropy in NT is defined as [Varotsos et al., 2006, 2011]:

$$S_{nt} = \sum_{k=1}^{N} p_k \chi_k \ln \chi_k - \left(\sum_{k=1}^{N} p_k \chi_k \right) \ln \left(\sum_{k=1}^{N} p_k \chi_k \right). \tag{6}$$

The entropy in NT is a dynamic entropy, depending on the order of the events [Varotsos et al., 2006]. Also, S_{nt-}, the entropy under time reversal, i.e., by reversing the order of the considered events (which of course changes the natural time used for the calculations), is also studied [Varotsos et al., 2006].

In many dynamical systems studied using the NT analysis method, it has been found that the value of κ_1 is a measure to quantify the extent of the organization of the system at the onset of the critical stage [Varotsos et al., 2011]. The criticality is reached when (a) κ_1 takes the value $\kappa_1 = 0.07$, and (b) at the same time both the entropy in NT and the entropy under time reversal satisfy the condition $S_{nt}, S_{nt-} < S_u = (\ln 2/2) - 1/4$ [Varotsos et al., 2011; Sarlis et al., 2011], where S_u is the entropy of the uniform distribution in NT [Varotsos et al., 2011, 2006].

In the special case of NT analysis of foreshock seismicity [Varotsos et al., 2001, 2005, 2006; Sarlis et al., 2008; Abe et al., 2005], we study the evolution of the quantities κ_1, S_{nt}, S_{nt-}, and $\langle D \rangle$ over time, where $\langle D \rangle$ is the "average" distance between the normalized power spectra $\Pi(\tilde{\omega})$ of the evolving seismicity, which is defined as:

$$\Pi(\tilde{\omega}) = \left| \sum_{k=1}^{N} p_k \exp(j\tilde{\omega}\chi_k) \right|^2, \tag{7}$$

and the theoretical estimation of $\Pi(\tilde{\omega})$ for $\kappa_1 = 0.07$:

$$\Pi_{critical}(\tilde{\omega}) \approx 1 - \kappa_1 \tilde{\omega}^2, \tag{8}$$

where $\tilde{\omega}$ stands for the angular frequency in NT.

Moreover, an "event" for the NT analysis of seismicity is considered to be any data point of the original seismicity time series (time series of magnitudes of EQs) that surpasses a magnitude threshold, M_{Thres}.

The analysis starts with an appropriately low threshold and taking into account only an adequate number of, "first in the order of occurrence", events. Next, the subsequent events, in their original order, are one-by-one taken into account. For each additional event that is taken into account, the quantity χ_k is rescaled within the interval (0,1] and all κ_1, S_{nt}, S_{nt-}, and $\langle D \rangle$ are re-calculated. This way, a temporal evolution of these quantities is obtained. The described procedure is repeated for several, increasing, values of M_{Thres} for each studied geographic area, and everything is repeated for different overlapping areas.

The seismicity is considered to be in a true critical state, a "true coincidence" is achieved, as soon as (a) κ_1 takes the value $\kappa_1 = 0.070$, (b) at the same time both the entropy in NT and the entropy under time reversal satisfy the condition $S_{nt}, S_{nt-} < S_u$, and three additional conditions are satisfied: (c) The "average" distance $\langle D \rangle$ should be smaller than 10^{-2}, i.e., $\langle D \rangle = \langle |\Pi(\tilde{\omega}) - \Pi_{critical}(\tilde{\omega})| \rangle < 10^{-2}$ (this is a practical criterion for signaling the achievement of spectral coincidence) [Varotsos et al., 2011]; (d) the parameter κ_1 should approach the value $\kappa_1 = 0.070$ "by descending from above", i.e., before the main event the parameter κ_1 should gradually decrease until it reaches the critical value 0.070 (this rule was found empirically) [Varotsos et al., 2001, 2011]; (e) the above-mentioned conditions (a)-(d) should continue to be satisfied even if the considered M_{Thres} or the area within which the seismicity is studied are changed (within reasonable limits).

The use of the magnitude threshold excludes some of the weaker EQ events (those events that their magnitude is $< M_{Thres}$) from the NT analysis. However, the usage of the magnitude threshold is valid for the reason that some recorded magnitudes are not considered reliable due to the seismographic network. On the other hand, the application of various M_{Thres} values are useful in determining the time range within which criticality is reached. This is because, in some cases, it is found that more than one time-points may satisfy the rest of the NT critical state conditions (a)-(d), and criterion (e) is the one that finally reveals the true time of criticality.

For the application of NT analysis to VLF data, we follow the paradigm of the NT analysis of seismicity, using the non-normalized VLF propagation quantities (defined in Section 3.1) to define the "energy" Q_k and the necessary threshold values as in [Potirakis et al., 2018a].

3.5 Method of critical fluctuations

It has been proposed that the EQ-related phenomena can be studied from the point of view of phase transition phenomena [Kawamura et al., 2012], characterized by the transition between two phases (states) in which a system could exist. Specifically, during the preparation of a main EQ the Earth's crust system sequentially experiences different states [Eftaxias et al., 2018]. MCF is a time series analysis method that is able to monitor the dynamics of the order parameter fluctuations; the critical dynamics, as well as the departure from the critical state, either by the emergence of tricritical dynamics or by appearance of the so-called "spontaneous symmetry breaking" (SSB) phenomenon [Contoyiannis et al. 2018; Potirakis et al., 2021, 2022]. MCF has been applied to a variety of time series which correspond to different observables of complex systems from many scientific fields, including

geophysical, biological, economic, thermal and electronics, [e.g., Potirakis et al., 2017, 2021; Kosmidis et al., 2018; Contoyiannis et al., 2004a, 2004b, 2021; Balasis et al., 2018; Zitis et al., 2022]. The application of MCF to various seismo-EM signals, including VLF sub-ionospheric propagation data, has been presented in detail in [Potirakis et al., 2021]. In the case of VLF sub-ionospheric propagation data, MCF is applied to the raw linear amplitude data (restored from the originally recorded dB values). In the following we briefly present the key notions of this method.

It has been shown that the dynamics of the fluctuations of the order parameter at the critical state can be modeled by the one-dimensional nonlinear intermittent map [Contoyiannis & Diakonos, 2000, 2007; Contoyiannis et al., 2002]:

$$\phi_{n+1} = \phi_n + u\phi_n^z + \varepsilon_n, \tag{9}$$

where ϕ_n is the n-th sample of the scaled order parameter, z is a characteristic exponent, and $u > 0$ is a coupling parameter. The shift parameter ε_n represents the non-universal uncorrelated noise. Also, it is mentioned that the exponent z for a thermal system is associated with the isothermal critical exponent δ as $z = \delta + 1$.

In the critical state, the plateau region of the invariant density $P(\phi)$ corresponds to the laminar region of the critical map where fully correlated dynamics takes place. The start of the laminar region is the fixed-point (f.p.) ϕ_0, determined by the edge of the most "abrupt" side of $P(\phi)$, while the end of the laminar region ϕ_L is not exactly defined [Potirakis et al., 2021]. Consequently, the parameter ϕ_L should be used as a varying parameter in the application of MCF.

An important observation in the application of MCF is the fact that the distribution $P(L)$ of the laminar lengths L, i.e., of the time intervals for which ϕ stays within the considered laminar region, (ϕ_0, ϕ_L), of a time series produced by the map of Equation (9) in the limit $\varepsilon_n \to 0$, is given by the power law-relation [Schuster, 1995]:

$$P(L) \sim L^{-p_L}. \tag{10}$$

Thus, the exponent p_L is $p_L = {}^{z}/_{(z-1)}$ and is connected with the isothermal exponent δ as $p_L = 1 + \left({}^{1}/_{\delta}\right)$. This power-law relation is related with the aforementioned plateau of the invariant density $P(\phi)$ and is a signature of the underlying correlated dynamics related to critical behavior [Contoyiannis et al., 2004b].

In detecting the critical state, the MCF focuses on revealing such power-laws and estimating the exponent p_L. For this purpose, a truncated power-law function $g(L)$ is used to model the $P(L)$ resulting for each considered ϕ_L:

$$g(L) = p_1 \cdot L^{-p_2} \cdot e^{-Lp_3}. \tag{11}$$

If $p_3 = 0$, then p_2 is equal to the exponent p_L of Equation (10). Since, from the theory of critical phenomena, the isothermal critical exponent δ is higher than 1 [Huang, 1987], and, as already mentioned, $z = \delta + 1$, $p_L = {}^{z}/_{(z-1)}$, for the critical state holds that $1 < p_L\ (=\ p_2) < 2$. Therefore, the critical state calls for the satisfaction of the conditions $p_2 > 1$ and $p_3 \approx 0$.

As already mentioned, the departure from the critical state, is signified either by the emergence of tricritical dynamics or by appearance of SSB. However, by means of the study of FEME/FEMR in the MHz band in analogy to thermal systems, it has most recently been found that post-SSB (and post-EQ) power-laws can be identified without being related to the preparation of a second main EQ [Potirakis et al., 2022]. Specifically, in a possible identification of post-SSB power-laws immediately after a very strong EQ, if the values of the autocorrelation function of the examined time series "collapse" immediately after the EQ and remain low, then no new strong EQ is expected, but if the autocorrelation function values return to high values, then a new strong EQ may be expected soon [Potirakis et al., 2022]. In the first case, the post-EQ power-laws in the distribution of laminar lengths, that are not accompanied by long memory in the corresponding autocorrelation function, are not related to a mainshock preparation processes but are associated to local fractures in course of the aftershock sequence which are not able to organize the system towards the preparation of a new mainshock [Potirakis et al., 2022].

4. Analysis of the lower ionosphere prior to "2021 Thessaly EQs"

In this section we present in detail the results obtained after analyzing the VLF subionospheric propagation data for the 2021 Thessaly EQs using the time series analysis methods that have been presented in Section 3. As mentioned in Section 2, we employed recordings of the UWA receiver, which is located in Athens, Greece, from seven VLF transmitters (see Fig.1), searching for pre-seismic signatures in the VLF amplitude data. This section comprises five subsections. Specifically, in Section 4.1 we present the results of the NFM statistical analysis that detect nighttime amplitude anomalies; in Section 4.2 we provide the sequential plots of the daily variation of VLF amplitude data, from which TTs anomalies are identified by inspection of the diurnal variation, while we also present the TTM statistical analysis results identifying anomalies in TTs, i.e., shifts of TTs. Section 4.3 reports the results of wavelet analysis, revealing AGW-related anomalies. Additionally, in Section 4.4 we present the NT analysis of the daily-valued non-normalized quantities (TR, DP and NF) of NFM analysis, uncovering approach to criticality, while n Section 4.5 we show the results of MCF analysis applied to the raw linear VLF amplitude recordings, uncovering the presence of critical dynamics.

4.1 NFM analysis results

In this section we present the results obtained by applying the Nighttime Fluctuation Method (NFM) (described in Section 3.1) to the VLF data of each one of the studied sub-ionospheric propagation paths (see Table 2). In this analysis we focus on the examined 2021 Thessaly EQs. In Fig. 4 we present an example of NFM analysis for the GBZ-UWA path (see Fig. 1), depicting the temporal evolution of the three NFM statistical quantities (TR^*, DP^*, NF^*). The standard deviation, σ, was calculated for the whole studied period starting from 2 February 2021 to 18 March 2021. The nighttime interval for application of NFM was chosen to be 21:30-02:05 UT for all analyzed paths (the 21:30-23:59 part corresponds to the "previous day" date, while the 00:00-02:05 UT part to the "next day" date). It should be noted that x-axis of Fig. 4 represents the date of the 00:00-02:05 UT part of the chosen

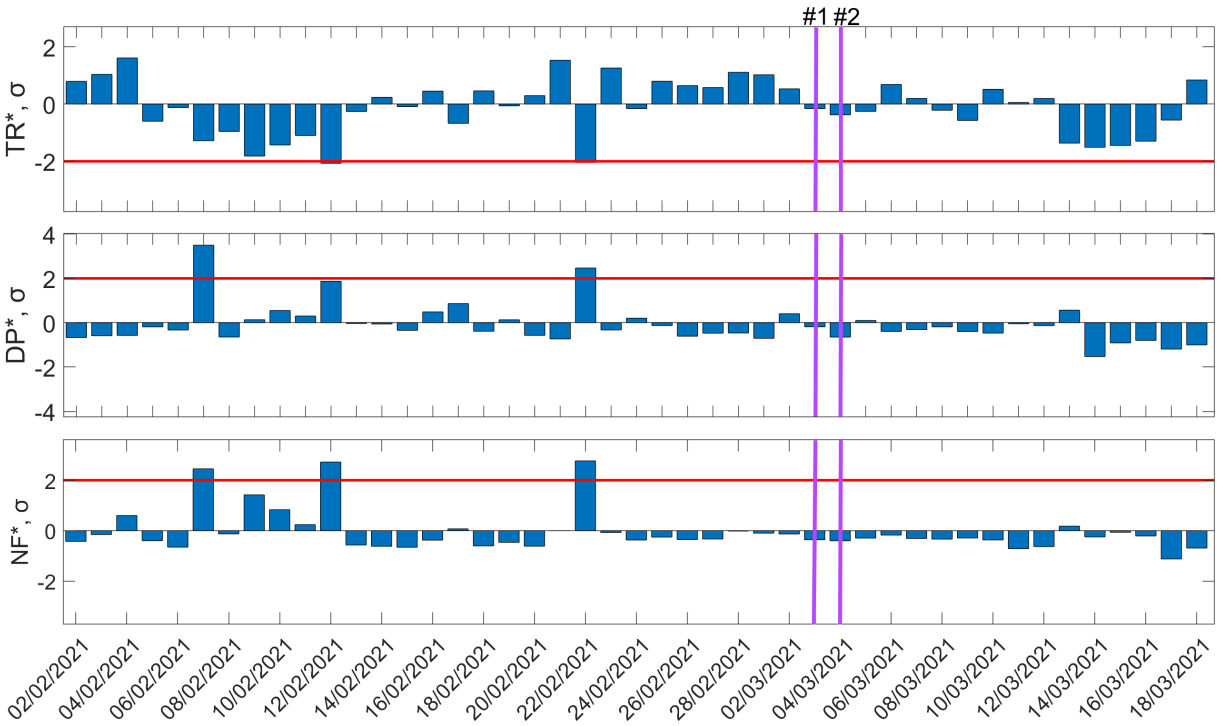

Figure 4. Temporal evolution of the three NFM normalized VLF propagation quantities for the GBZ-UWA propagation path: TR^* (top panel), DP^* (middle panel), and NF^* (bottom panel). Red solid horizontal lines indicate the corresponding $-2\sigma/+2\sigma$ thresholds; σ for each panel was calculated for the whole studied period. The dates of occurrence of the two 2021 Thessaly EQs are marked in each panel with two solid vertical purple lines.

Date of the Appearance of the Anomaly	*TR**	*DP**	*NF**	Possibly Associated Extreme Event(s)
02 February 2021		DHO		a
03 February 2021		NRK		a, b
07 February 2021	HWU, ICV	GBZ, ICV	GBZ, HWU, ICV	a
08 February 2021	ICV	ICV	HWU, ICV	a
09 February 2021	NRK	ICV	ICV, NRK	a, b
10 February 2021	ICV		ICV	a
12 February 2021	GBZ		FTA, GBZ	a
14 February 2021	JXN		JXN	a
15 February 2021		HWU		a
16 February 2021		JXN	JXN	a
21 February 2021		DHO		c
22 February 2021	GBZ	GBZ	GBZ	c
25 February 2021	NRK	NRK	NRK	c
28 February 2021		DHO		c
3 March 2021			DHO	c
11 March 2021		HWU		d
12 March 2021	NRK			e
13 March 2021			NRK	e
14 March 2021		ICV		f
15 March 2021	ICV	ICV	HWU, ICV	f
16 March 2021	HWU		HWU	f

The following letters appearing in the column "Possibly associated extreme event(s)" denote, respectively: a→ a 5.5 M_w EQ that occurred on 17 February 2021 03:36:07 (UT) at (38.406°N, 22.019°E); b→ a 5.6 M_w EQ that occurred on 24 February 2021 13:47:55 (UT) at (63.949 °N 22.285 °W), likely only affects the NRK-UWA sub-ionospheric propagation path; c→ 1st 2021 Thessaly EQ (6.3 M_w, 3 March 2021); d→ a 5.6 M_w EQ that occurred on 12 March 2021 12:57:50 (UT) at (39.893 °N 22.088 °E); e→ Fagradalsfjall volcano with unknown VEI erupted on 19 March 2021; f→ a 5.5 M_w EQ that occurred on 27 March 2021 13:47:55 (UT) at (42.448°N, 16.050°E).

Table 3. NFM analysis results. Anomalies in any of the three NFM statistical quantities (TR^*, DP^*, NF^*) (exceeding the corresponding $-2\sigma/+2\sigma$ threshold) are denoted by the call name of the transmitter(s) of the perturbed path(s) for which these were identified.

nighttime interval, i.e., the "next day" date. This was decided on the basis that the local time was LT = UT+2 h, so the LT nighttime part is shifted to the "next day" date, rendering the "next day" LT nighttime part longer than its "previous day" counterpart. It is also mentioned that all paths' data were carefully checked for periods of long VLF signal absence or even short disruptions and any nighttime excerpt containing them was not included in the NFM calculations. Thus, only the natural fluctuations of the nighttime amplitude of the signal were taken into account.

In applying NFM, anomalies, exceeding the $\pm 2\sigma$ thresholds, in each statistical quantity are usually considered as possibly correlated with the EQs under study when found within a time interval of 15 days prior to each of the studied EQs. As evident from Fig. 4, an important anomaly is simultaneously found in all three statistical parameters (exceeding $\pm 2\sigma$ thresholds) on 22 February 2021 (see also Table 3). Since this anomaly is 9 (< 15) days ahead of the occurrence of the first 2021 Thessaly EQ, is considered probably related with it. Also, as we can see from Fig. 4, there are two more anomalies on 7 and 12 February 2021, the first in DP^* and NF^*, and the second in TR^* and NF^*. However, these anomalies are not considered correlated with the examined EQs due to their long (>15 days) time distance from them. However, these could be attributed to a 5.5 M_w EQ which occurred in Phocis, Greece, on 17 February 2021 (mentioned in Section 2).

Table 3 summarizes all statistical anomalies identified, for any of the three normalized daily-valued VLF propagation quantities TR^*, DP^* and NF^*, in any of the studied paths, from 2 February 2021 to 18 March 2021. The path for which each of these anomalies was found, is indicated by the corresponding transmitter call name in the cell belonging to the line of the anomalous date and the column of the corresponding VLF propagation quantity which exceeded the corresponding $+2\sigma/-2\sigma$ threshold. The last column of Table 3 attributes each anomaly either to the examined 2021 Thessaly EQs, or to any other possibly ionosphere-influencing extreme event (another EQ or other kind of extreme event). It is noted that, several anomalies were found (at different dates, <15 days) prior to the 1st 2021 Thessaly EQ for the DHO-UWA, GBZ-UWA and NRK-UWA sub-ionospheric propagation paths, while no anomaly was found after the 1st and before the 2nd 2021 Thessaly EQ, due to the short time distance (~1 day) between the two examined EQs and the fact that NFM examines daily-valued statistical quantities. The above-

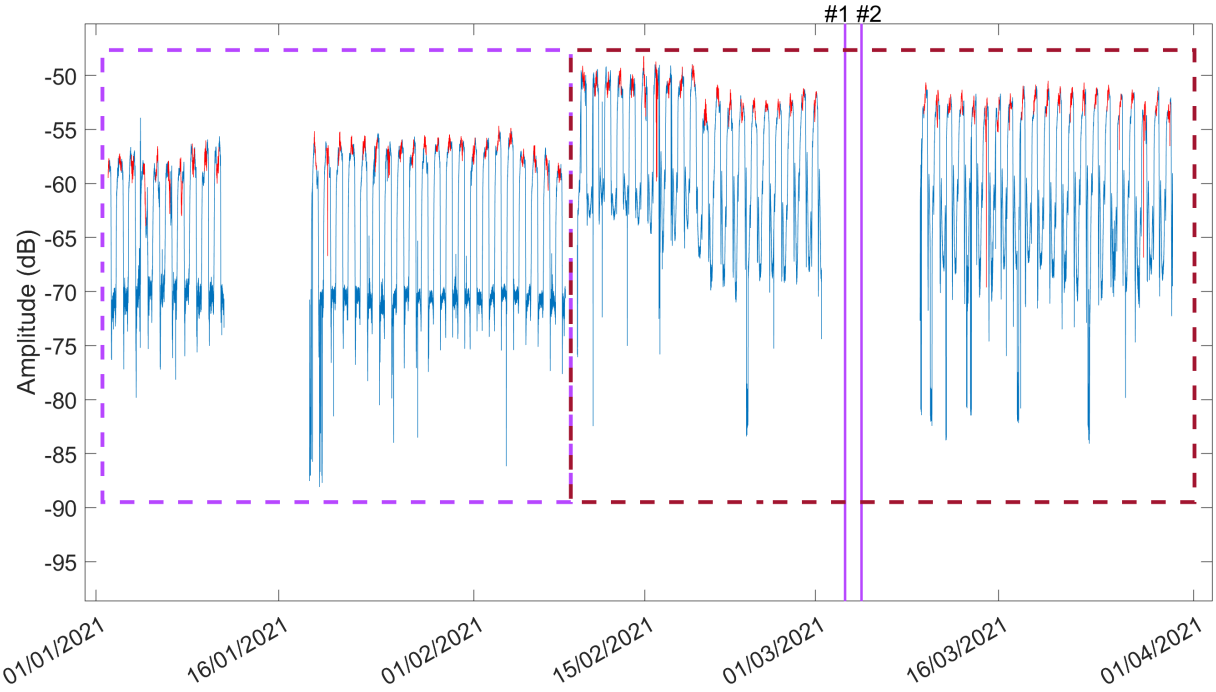

Figure 5. Diurnal variation of HWU-UWA subionospheric propagation path starting from 2 January 2021 until 30 March 2021. Parts of the recordings during which there was absence of signal (the transmitter was off) have been removed (void parts on the plot). The nighttime parts of the amplitude recordings (21:30-02:05 UT) are shown with red color, while the two dashed orthogonals (the purple- and the brown-colored, in the left and the right side of the plot, respectively) classify the signal into two epochs. The two solid vertical purple lines indicate the occurrence time (see Table 1) of the two EQs under study. Significant difference in the mean amplitude level is observed between these two epochs, which is considered to be a transmitter-operation-related anomaly.

mentioned anomalies are considered more probably correlated with the 1st 2021 Thessaly EQ. As one can see from Table 3, other anomalies which are considered not associated with the examined EQs, are attributed to other possibly ionosphere-influencing extreme events that have been mentioned in Section 2 (mostly other EQs).

It should finally be mentioned here that a specific preprocessing has been applied (only) to the nighttime amplitude fluctuations of the HWU-UWA subionospheric propagation path, in order to apply the NFM without its results to be influenced by transmitter-operation-related anomalies. Figure 5 depicts an example of the recordings from HWU within which the analyzed time period falls. Specifically, the time window from 2 January 2021 to 30 March 2021 is shown. Note that the void parts correspond to absence of signal. For the specific time periods only noise was recorded, which is not shown in this plot, while the corresponding nighttime parts of these recordings were not used in the NFM analysis. The nighttime amplitude recordings (21:30-02:05 UT) are depicted in the diurnal variation of the signal with red color. From Fig. 5, it is evident that the recordings marked with the right-hand-side orthogonal (brown-colored, dashed) of the diurnal variation of the signal are of significantly higher amplitude level than the recordings marked with the left-hand-side orthogonal (purple-colored, dashed), leading to a significant difference in their mean amplitude levels, which, if not compensated, would be revealed as an anomaly by NFM, although it is clearly transmitter-operation-related. In order to compensate this, the NFM-influencing difference in the amplitude level of these two epochs was found by initially calculating the mean values of the first and the second epoch using only the nighttime amplitude data. Subsequently, by subtracting the mean value of the second epoch from the mean value of the first epoch, an offset has been computed, which is then added to the first epoch's recordings. After this compensation, the NFM was, as usually, applied to the nighttime amplitude data of the analyzed time period.

4.2 Diurnal variation and TTM analysis results

This section presents the sequential plots of the diurnal variation of the amplitude of the filtered (by a Gaussian filter) VLF signals, with terminator times (TTs) noted, as well as the results of the terminator time method (TTM) analysis. First, we detected the position of TTs by locating the minima in the daily VLF amplitude recordings, while as a second step we applied the TTM, as described in Section 3.2.

Figure 6 portrays an example of the diurnal variations of the filtered amplitude data for the propagation path GBZ-UWA, in the form of stacked 24 h signals, shifted by 10 dB/day. The time axis spans 24 h (in UT) and the presented time period is 16 February 2021 – 7 March 2021, including 15 days prior to the 2021 Thessaly EQs, while the date to which each curve corresponds are shown in the middle of each of diurnal variation of the signal, and the dates of occurrence of the examined EQs are marked with orange color. The minima of the amplitude close to the local (planetary) sunrise and sunset times are identified as morning TTs (t_m) and the evening TTs (t_e), respectively, and are shown in Fig. 6 with that order from left to right (denoted red and green color, respectively). The anomalous shifts of those minima observed for different days prior to the 2021 Thessaly EQs, are marked with black ellipses, including the previous and the next normal days around each anomaly. It is noted that some of the studied paths presented multiple minima close to the sunrise and/or sunset times. In these cases, we used the ones closest to the daytime part of the signal. Moreover, in some path cases, one of the terminator times was not easily identifiable due to small difference of the minimum and the adjacent daytime and nighttime parts of the signal. In these cases, we chose to skip the analysis of the specific terminator time, as well as of the VLF-daylength.

As already mentioned, after locating the TTs, we proceeded in applying the TTM method to identify any statistical anomalies in the TTs or the VLF-daylength. Figure 7 depicts an example of TTM results for the ICV-UWA sub-ionospheric propagation path. In this figure we show the obtained shifts in the morning TTs, denoted as dt_m, in the evening TTs, dt_e, and in the VLF-daylength, dD_{VLF}, all calculated as described in Section 3.2. The standard deviation, σ, of each analyzed time series has been calculated for the whole studied period starting from 2 February of 2021 until 18 March of 2021, whereas the corresponding $\pm 2\sigma$ levels are shown in each panel. Possible pre-seismic anomalous shifts of TTs which are denoted as "excesses" of the abovementioned limits have been found prior to the two examined EQs in the evening TT on 24 February 2021 by exceeding the $+2\sigma$ limit (t_e shifted by +22.06 min), as well in the VLF-daylength, D_{VLF} shifted by −22.6 min (exceeding the -2σ threshold). These anomalies are possibly attributed to the 1st 2021 Thessaly EQ. Other anomalies identified in the specific path were found in different dates and are considered to be due to other EQs (see also Table 4). Specifically, the statistical anomalies found in 6, 7 and 13 February are possibly associated with the 5.5 M_w EQ that occurred on 17 February 2021 03:36:07 (UTC)

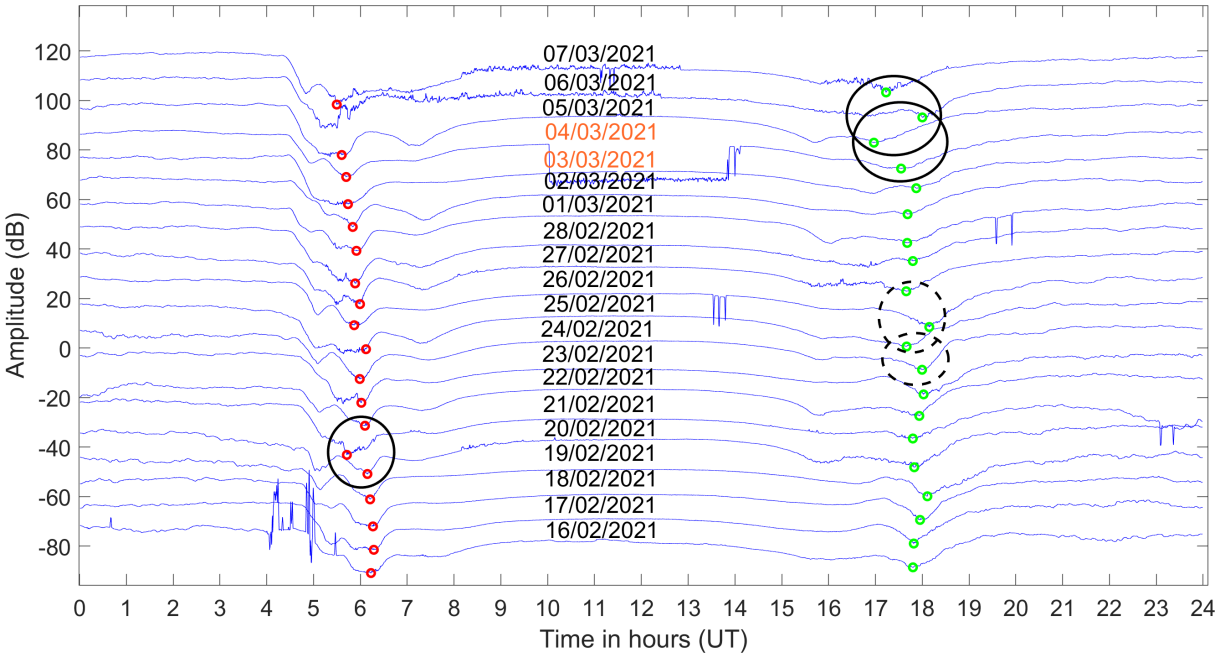

Figure 6. Diurnal variation of the amplitude of the VLF signal for the propagation path GBZ-UWA for the time period 16 February 2021 – 7 March 2021. Each signal is vertically shifted by +10 dB in regards to the signal of the previous day. The first appearing minima (before sunrise), marked with red circles, are identified as the morning TTs t_m, while the evening TTs t_e are marked as green circles. Finally, the dates of the two 2021 Thessaly EQs are marked with orange color. The black ellipses indicate the existence of shifts of TTs. Ellipses with solid circumference indicate anomalies which were statistically confirmed by the application of the TTM (see also Table 4), while the dashed circumference ellipses indicate anomalies that were found statistically insignificant according to TTM (not exceeding $\pm 2\sigma$ thresholds) and thus don't appear in Table 4.

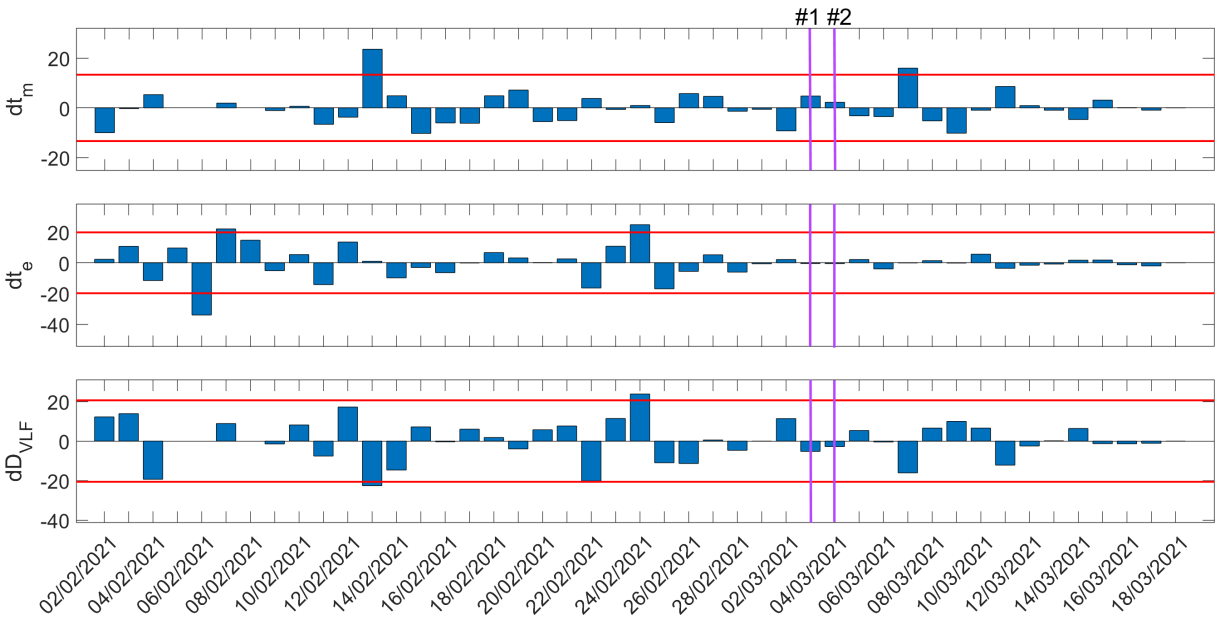

Figure 7. Temporal evolution of the shifts in the morning and evening TTs, as well as in the VLF-daylength for the propagation path ICV-UWA during the studied period, from 2 February 2021 to 18 March 2021. Red solid horizontal lines indicate the corresponding $\pm 2\sigma$ thresholds; σ for each panel was calculated for the whole studied period. The dates of occurrence of the two 2021 Thessaly EQs are marked in each panel with two solid vertical purple lines.

at (38.406°N, 22.019°E), while the 7 March anomaly is probably associated with the 5.6 M_w EQ of 12 March 2021 12:57:50 (UT) at (39.893 °N 22.088 °E).

Table 4 summarizes all the anomalies (exceeding of the threshold levels $\pm 2\sigma$) revealed by the TTM analysis of the studied subionospheric propagation paths, for time period for which the NFM analysis was applied (see Section 4.1). Table 4 follows the format of Table 3, while, additionally, the anomalous shifts of TTs (in min) are also mentioned for each anomaly. Table 4 presents information about the morning and evening TTs, as well as the calculated VLF-daylength. As it is evident from Table 4, terminator time analysis was possible only for five of the seven studied paths, while in three of them, namely in the GBZ-UWA, ICV-UWA and DHO-UWA paths, were detected four TTs' statistical anomalies which are possibly associated with the examined 2021 Thessaly EQs. Nevertheless, all revealed TTs statistical anomalies can be explained in terms of EQ events that occurred along the examined paths.

Date of Appearance of the Anomaly	Excess of $\pm 2\sigma$ for dt_m	Excess of $\pm 2\sigma$ for dt_e	Excess of $\pm 2\sigma$ for D_{VLF}	Possibly Associated Extreme Event(s)
5 February 2021	NRK (shift −13.61 min)			a
6 February 2021		ICV (shift −34.00 min)		a
7 February 2021		ICV (shift +22.06 min) GBZ (shift +38.15 min)	GBZ (shift +36.95 min)	a
8 February 2021	HWU (shift −12.35 min)			a
10 February 2021	HWU (shift +14.95 min)			a
13 February 2021	ICV (shift +23.58 min)		ICV (shift −22.60 min)	a
21 February 2021	GBZ (shift −19.59 min)			b
24 February 2021		ICV (shift +24.79 min)	ICV (shift −23.83 min)	b
3 March 2021	DHO (shift +13.41 min)			c
5 March 2021	DHO (shift −12.38 min)	GBZ (shift −33.39 min)		d
6 March 2021		GBZ (shift +33.93 min)		d
7 March 2021	ICV (shift +15.98 min)			d
18 March 2021		GBZ (shift −32.55 min)	GBZ (shift −27.58 min)	e
The following letters appearing in the column "Possibly associated extreme event(s)" denote, respectively: a→ a 5.5 M_w EQ that occurred on 17 February 2021 03:36:07 (UTC) at (38.406°N, 22.019°E); b → 1st 2021 Thessaly EQ (6.3 M_w, 3 March 2021); c→ 2nd 2021 Thessaly EQ (5.8 M_w, 4 March 2021); d→ a 5.6 M_w EQ that occurred on 12 March 2021 12:57:50 (UT) at (39.893 °N 22.088 °E); e→ a 5.5 M_w EQ that occurred on 27 March 2021 13:47:55 (UTC) at (42.448°N, 16.050°E)				

Table 4. TTM analysis results. Anomalies in any of the TTs or the the VLF-daylength (exceeding the corresponding $\pm 2\sigma$ thresholds) are denoted by the call name of the transmitter(s) of the perturbed path(s) for which these were identified.

4.3 Wavelet Analysis Results

In this section we present the results of the wavelet analysis of the studied paths' VLF amplitude recordings, searching for any of wave-like structures that fall within the cone of influence (CoI) of the scalogram. The procedure followed is described in Section 3.3. For the wavelet analysis of each path, we used the same nighttime interval (21:30-02:05 UT) as used for NFM analysis (see Section 4.1). Possible anomalies, appearing as wave-like structures which are depicted as wavelet power increases in the scalogram, identified within a time period of 15 days prior to each of the studied EQs, are considered as pre-EQ AGWs before the 2021 Thessaly EQs.

An example of wavelet analysis for the GBZ-UWA path is shown in Fig. 8, where each analyzed part of nighttime amplitude recordings, starting from 17 February of 2021 until 4 March of 2021, is shown in a separate panel (16 panels are displayed), whereas the two dates marked with red color refer to each of the examined 2021 Thessaly EQs date of occurrence. Figure 8 reveals that clear wave-like anomalies (increases in the power of the scalogram inside the CoI) at low periods, implying AGWs, were present at different dates on 17-24 February 2021 (maximum intensification on 22-24 February 2021), a few days before the 1st 2021 Thessaly EQ.

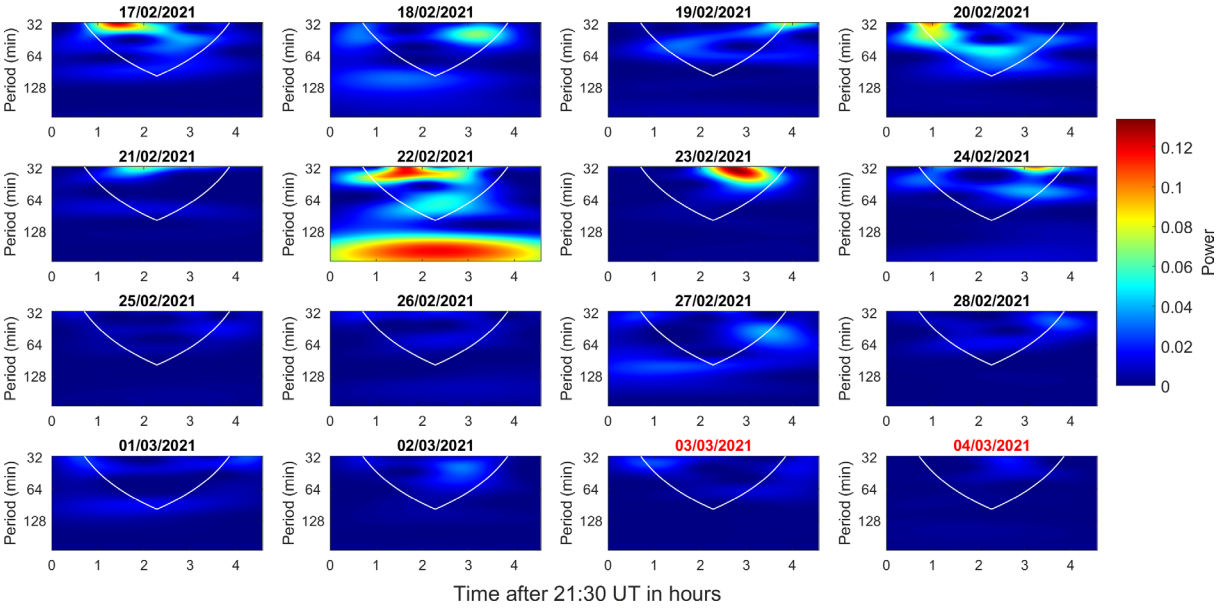

Figure 8. Nighttime scalograms of the GBZ-UWA sub-ionospheric propagation path for the time period from 17 February 2021 to 4 March 2021. The two dates of occurrence of the 2021 Thessaly EQs are red-colored; the horizontal axis of each panel refers to the considered nighttime interval 21:30- 02:05 UT, while 0 h corresponds to previous date's 21:30 UT. The white curves denote the Cones of Influence (CoI). Vertical axis refers to wavelet scale (or "period") and the color information corresponds to wavelet power (linear scale).

Table 5 summarizes the identified scalogram anomalies, indicating AGWs, grouped by path (indicated by the call name of the transmitter) in which they were found. For each identified wave-like structure, its time of appearance, period's range (in minutes), and intensity are provided alongside with its date of occurrence. Finally, the last column attributes each wavelet anomaly either to the examined 2021 Thessaly EQs, or to any other possibly ionosphere-influencing extreme event. It is noted that due to the fact that the 2021 Thessaly EQs occurred with ~1 day difference, all AGW indications revealed before 3 March 2021 were attributed to the 1st 2021 Thessaly EQ, while the only AGW indication that was found after the 1st and before the 2nd 2021 Thessaly EQ (in the NRK-UWA path, on 3 March 2021, 22:12:36 UT – 22:34:48, UT) was attribute to the 2nd 2021 Thessaly EQ. Other EQs that occurred along the examined paths are also indicated as possibly associated to the revealed AGWs.

Lower-ionosphere anomalies prior to strong earthquakes in north-central Greece on March 2021

Transmitter	Date of the Appearance of the Anomaly	Time of Appearance of the Anomaly (UT)	Range of Periodic Structures (min)	Intensity of the Wave-Like Structures	Possibly Associated Extreme Event(s)
NRK	21 February 2021	00:15:00 – 01:04:48	31 – 38	high	a
	24-25 February 2021	22:13:48 – 00:33:36	31 – 38	moderate	b
	2-3 March 2021	22:15:00 – 01:15:00	31 – 36	moderate	b
	3 March 2021	22:12:36 – 22:34:48	31 – 38	moderate	c
JXN	19 February 2021	22:13:48 – 22:24:00	31 – 36	high	b
	24 February 2021	22:39:00 – 23:24:36	31 – 38	moderate	b
GBZ	16 February 2021	22:30:36 – 23:24:36	31 – 36	high	b
	17-18 February 2021	00:06:00 – 01:07:48	36 – 47	moderate	b
	19 February 2021	01:00:36 – 01:21:00	31 – 36	moderate	b
	19 February 2021	22:13:48 – 22:39:00	31 – 36	moderate	b
	20 February 2021	23:01:48 – 00:00:00	31 – 36	moderate	b
	21-22 February 2021	22:24:00 – 00:13:48	31 – 41	high	b
	22-23 February 2021	23:46:48 – 00:52:48	31 – 41	high	b
	24 February 2021	00:30:00 – 00:58:48	31 – 33	high	b
	16 March 2021	00:52:59-01:33:00	31 – 38	moderate	e
ICV	18-19 February 2021	23:09:36 – 00:24:36	44 – 66	high	b
	19 February 2021	22:31:48 – 23:12:00	31 – 33	high	b
FTA	17 February 2021	23:09:00 – 23:54:00	31 – 36	high	b
	19-20 February 2021	23:33:00 – 00:06:00	31 – 36	moderate	b
	21 February 2021	23:46:28 – 23:55:48	50 – 66	moderate	b
	22 February 2021	00:33:36 – 01:21:00	31 – 38	high	b
	5-6 March 2021	23:03:36 – 00:15:36	44 – 62	moderate	d
	11 March 2021	00:06:36 – 00:43:48	31 – 36	moderate	d

Transmitter	Date of the Appearance of the Anomaly	Time of Appearance of the Anomaly (UT)	Range of Periodic Structures (min)	Intensity of the Wave-Like Structures	Possibly Associated Extreme Event(s)
HWU	19 February 2021	23:12:36 – 23:57:36	31 – 33	high	b
	20-21 February 2021	22:58:48 – 00:04:48	31 – 44	high	b
	22 February 2021	00:12:36 – 00:48:00	31 – 36	high	b
	14 March 2021	22:28:59 – 23:15:59	41 – 58	moderate	e
DHO	17 February 2021	22:24:00 – 23:06:00	31 – 38	high	b
	27-28 February 2021	22:21:00 – 00:37:48	31 – 47	moderate	b
	28 February 2021	22:12:36 – 22:39:36	31 – 44	high	b
	5 March 2021	22:39:00 – 23:46:48	35 – 58	moderate	d
	9-10 March 2021	23:30:00 – 00:42:00	41 – 44	moderate	d
	11 March 2021	00:03:00 – 01:10:48	35 – 44	high	d
	12 March 2021	22:12:36 – 22:30:00	31 – 35	high	e

The terms "high" and "moderate" in the column "Characterization of the intensity of power of the wave-like structures" verbally characterize the intensity of the wave-like structures with reference to the normalized linear scale of power (33-66% for "moderate" and 67-100% for "high"). The following letters appearing in the column "Possibly associated extreme event(s)" denote, respectively: a→ a 5.6 M_w EQ that occurred on 24 February 2021 13:47:55 (UT) at (63.949 °N 22.285 °W), likely only affects the NRK-UWA sub-ionospheric propagation path; b→ 1st 2021 Thessaly EQ (6.3 M_w, 3 March 2021); c→ 2nd 2021 Thessaly EQ (5.8 M_w, 4 March 2021); d→ a 5.6 M_w EQ that occurred on 12 March 2021 12:57:50 (UT) at (39.893 °N 22.088 °E); e→ a 5.5 M_w EQ that occurred on 27 March 2021 13:47:55 (UTC) at (42.448°N, 16.050°E).

Table 5. Wavelet analysis results for the studied sub-ionospheric propagation paths. Increases of the wavelet power at specific scales denote the existence of "wave-like structures" indicating the existence of AGWs.

4.4 Natural time (NT) Analysis Results

In this section we present the results obtained after the application of the NT analysis method (see Section 3.4) to the daily-valued time series of the NFM analysis non-normalized VLF propagation quantities *TR*, *DP*, and *NF* (see Section 3.1). We have applied the NT method to the above-mentioned VLF sub-ionospheric propagation data as already successfully applied in other significant EQ cases [Potirakis et al., 2018a, 2021; Politis et al., 2021]. Specifically, for each one of the aforementioned VLF propagation quantities, we consider as an event any daily value of the VLF quantity under analysis, that is higher than a certain threshold, consequently excluding values which are weaker than the specific threshold. Then, the "energy" Q_k of the k-th revealed event is considered to be equal to the corresponding daily value of the analyzed VLF propagation quantity. Finally, the NT analysis is applied to the time series of the revealed events of each VLF propagation quantity, as in the case of the pre-EQ seismic activity (see Section 3.4 and [Potirakis et al., 2018a, 2021]).

Here, we are looking for criticality signatures that are associated with the 2021 Thessaly EQs in the three statistical quantities TR, DP, and NF of each one of the studied of the seven sub-ionospheric propagation paths (see Table 2). Figure 9 presents an example of such an NT analysis, portraying the results obtained for the *NF* VLF propagation quantity of the DHO-UWA path for the examined time period (from 2 February of 2021 to 18 March of 2021). As one can see from Fig. 9 the NT criticality criteria were satisfied on 1 March 2021, since on that date, simultaneously, κ_1 approaches the value $\kappa_1 = 0.070$ "by descending from above", $S_{nt}, S_{nt-} < S_u$ and $\langle D \rangle < 10^{-2}$ for all four presented NF_{Th} threshold values (see also Section 3.4). The magenta patches in Fig. 9 show the time periods during which the approach to criticality was found for each NF_{Th}, while their intersection reveals that "true coincidence", i.e., true critical state (see Section 3.4), was achieved on 1 March 2021, which is 2 days before the 1st 2021 Thessaly EQ with which the identified criticality is considered to be associated.

It should be clarified that the $(\mathrm{Dst})_{\min} = -58$ nT geomagnetic storm of 1 March 2021 (06:00 UT) (see Fig. 3 in Section 2) is considered unlikely to be associated with the specific criticality signature for the following reasons: (a) Critical state always precedes the associated extreme event. Thus, when the time step of the analyzed time series is 1 day, as happens for the analyzed non-normalized VLF propagation quantities of NFM, any approach to criticality revealed by the NT analysis cannot be considered as possibly associated with an extreme event unless identified at least 1 day before the extreme event; in the specific case, criticality was found on the same day that the aforementioned magnetic storm occurred, so the specific criticality signature cannot be associated with it. (b) Even if criticality was identified before 1 March 2021, the effect of the preparation of the specific weak magnetic storm, marginally classified even as minor, on the lower ionosphere is considered negligible compared to the effect of 1st 2021 Thessaly EQ (epicenter on land, $M_w = 6.3$, depth = 8 km, close to the receiver) on the lower ionosphere. Note also that past studies advocate the view that such a weak magnetic storm could not affect Ionosphere's D layer and, thus, could not be detectable through a VLF receiver's amplitude, [e.g., Kumar & Kumar, 2014; Maurya et al., 2016;

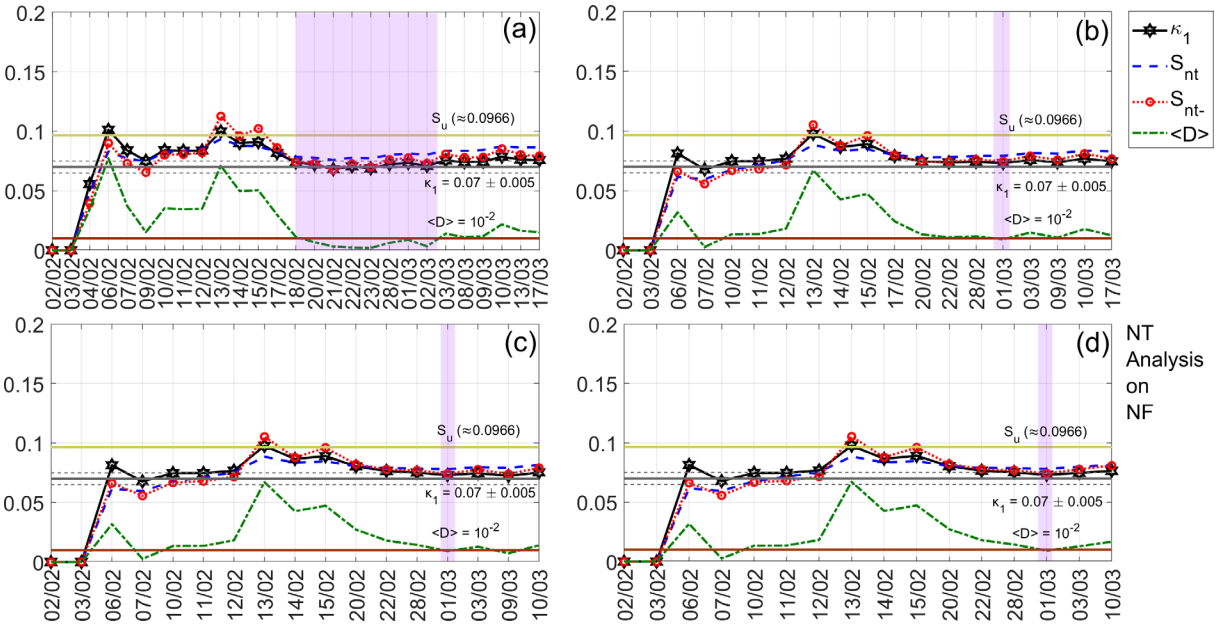

Figure 9. NT analysis of the *NF* VLF propagation quantity time series of the propagation path DHO-UWA for the examined period, from 2 February 2021 to 18 March 2021. The presented temporal variations of the NT parameters correspond to the different thresholds of NF_{Th}: (a) 18000, (b) 34000, (c) 38000, (d) 40000, respectively. The limit value of the entropy $S_u(\approx 0.0966)$ appears as a horizontal solid light green line, while the κ_1 value 0.07 along with a region of ± 0.005 around it, are denoted by a horizontal solid grey and two horizontal dashed grey lines, respectively. The 10^{-2} $\langle D \rangle$ threshold is shown as a horizontal brown line. The events presented in each panel depend on the corresponding NF_{Th}. Moreover, although the conventional time (date) of the occurrence of each corresponding event is noted in the x-axis tick values, the x-axis scale actually follows the NT representation; for this reason, the x-axis is not linear in conventional time. Date format is Day/Month, while for all the dates the Year is the same: 2021.

Date of the appearance of criticality	NT analysis on TR	NT analysis on DP	NT analysis on NF	Possibly Associated Extreme Event(s)
15 February 2021			FTA	a
17 February 2021	FTA		HWU, GBZ, FTA	b
18 February 2021			FTA	b
22 February 2021	HWU, ICV			b
23 February 2021		JXN	GBZ	b
24 February 2021			GBZ	b
25 February 2021	ICV		HWU, JXN, GBZ	b
26 February 2021	ICV		HWU	b
27 February 2021	ICV			b
28 February 2021	JXN, ICV	HWU		b
1 March 2021	ICV	HWU, JXN, NRK	DHO	b
2 March 2021	ICV			b
3 March 2021			NRK	c
6 March 2021		FTA		d
8 March 2021			FTA	d
9 March 2021			FTA	d
10 March 2021		NRK		d
12 March 2021		FTA		e
16 March 2021		FTA		e
17 March 2021			FTA	e
The following letters appearing in the column "Possibly associated extreme event(s)" denote, respectively: a→ a 5.5 M_w EQ that occurred on 17 February 2021 03:36:07 (UT) at (38.406°N, 22.019°E); b→ 1st 2021 Thessaly EQ (6.3 M_w, 3 March 2021); c→ 2nd 2021 Thessaly EQ (5.8 M_w, 4 March 2021); d→ a 5.6 M_w EQ that occurred on 12 March 2021 12:57:50 (UT) at (39.893 °N 22.088 °E); e→ a 5.5 M_w EQ that occurred on 27 March 2021 13:47:55 (UTC) at (42.448°N, 16.050°E).				

Table 6. NT analysis results. The revealed approaches to criticality are denoted by the call name of the transmitter(s) of the path(s) for which NT analysis criticality conditions were found to be satisfied.

Zhao et al., 2020; Das et al., 2021]. Nevertheless, we tried to further check this, by checking the VLF recordings of the ISR-UWA path (ISR is a VLF transmitter which is located in Negev, Israel, (37.4094° N, 27.3252° E), with operation frequency 29.7 kHz), which is almost in the opposite direction, and the TBB-UWA path (TBB is a VLF transmitter which is located in Denizköy, Turkey, (37.4094° N, 27.32527° E), with operation frequency 26.7 kHz), which is in almost perpendicular direction to the examined paths. Since a geomagnetic storm is a global phenomenon, any criticality identified in VLF data before a geomagnetic storm should be identified for all propagation paths. However, unfortunately, none of these paths' recordings were appropriate for analysis due to poor function of the corresponding transmitters during the time period of interest.

Table 6 summarizes all criticality indications identified by the NT analysis, for any of the three non-normalized VLF propagation quantities of TR, DP and NF, in any of the studied paths, from 2 February 2021 to 18 March 2021 (the same time period for which the NFM results have been presented in Section 4.1). The path for which each of these criticality indications was found, is marked by the corresponding transmitter call name in the cell belonging to the line of the criticality date and the column of the corresponding VLF propagation quantity in which criticality was identified. The last column of Table 6 attributes each anomaly either to the examined 2021 Thessaly EQs, or to any other possibly ionosphere-influencing extreme event. Note that the paths JXN-UWA and HWU-UWA was not possible to be analyzed beyond 1 March 2021, because on 2 March they presented loss of signal (until 8 and 9 March 2021, respectively), because simple skipping of the dates for which these transmitters were down would disturb the dynamics of the events considered for the NT analysis, leading to false results after 2 March 2021. Nonetheless, it has to be stressed that the NT analysis results obtained for the specific paths that revealed criticality before 2 March are still reliable.

It is clear from Table 6 that criticality was detected in different VLF propagation quantities and dates, but in all studied paths, within 15 days before the 1st 2021 Thessaly EQ. As mentioned above, when commenting on the NT analysis example of Fig. 9, critical state always precedes the associated extreme event. Thus, any criticality associated with the 2nd 2021 Thessaly EQ, should be identified at least 1 day before the specific EQ, i.e., on 3 March 2021 or earlier, while for the 1st 2021 Thessaly EQ these should appear on 2 March or earlier. So, only the criticality identified for the NRK-UWA path on 3 March 2021 can be undoubtably attributed to the 2nd 2021 Thessaly EQ. For this reason, all criticality indications identified before are considered more probably correlated with the 1st 2021 Thessaly EQ. Finally, as shown in Table 6, the ionosphere also reached criticality on 15 February 2021, as well as on 6, 8, 9, 10, 12, 16 and 17 March 2021 which are likely associated with other ($M \geq 5.5$) EQs that occurred along the paths for which the NT criticality criteria were satisfied.

4.5 MCF Analysis Results

In this section we present the results obtained for the VLF amplitude recordings of all the examined subionospheric propagation paths (see Section 2) using the method of critical fluctuations (MCF), by following the steps of the method as described in Section 3.5. We should clarify that the daily-valued VLF propagation quantities of NFM, which have been analyzed by means of the NT analysis, cannot be analyzed by means of the MCF for the reason that their time series comprise very few values, whereas the MCF needs > ~5000 values in order to produce reliable results [Potirakis et al., 2021]. The MCF is applied to the raw linear amplitude of the nighttime fluctuation data, obtained from the originally recorded amplitude level values (in dB). More specifically, MCF is applied to time windows (i.e., excerpts) of the VLF amplitude recordings time series that present stationarity, provided that transmitter's signal is present (as in the analysis methods presented above, periods of long VLF signal absence or even short disruptions and any nighttime excerpt containing them was not analyzed using MCF). In case that MCF criticality conditions were found to be satisfied, the analyzed time window is referred to as "critical window" (CW). We exhaustively searched for such kind of excerpts in the recordings of each one subionospheric propagation path prior to each of the 2021 Thessaly EQs.

Figure 10 portrays an example of MCF analysis for the CW identified in ICV-UWA path recordings of 2 March of 2021, i.e., ~1 day prior to the 1st 2021 Thessaly EQ. More specifically, in Fig. 10a we show an 16,400 s sample-long excerpt (70,000 s – 86,400 s, i.e., 2 March 2021 19:26:39-23:59:59 UT). The corresponding distribution of the specific time excerpt is presented in Fig. 10b, where the selected fix point (f.p.), i.e., the ϕ_0 value (start of laminar regions), for the MCF analysis is indicated (see Section 3.5). As mentioned in Section 3.5, during the application of MCF the parameter ϕ_L (end of laminar region) is used as a varying parameter. It is also reminded that the intervals between

ϕ_0 and each one of the ϕ_L values define the corresponding laminar regions (ϕ_0, ϕ_L) — that is, one laminar region (ϕ_0, ϕ_L) for each different ϕ_L value. In Fig. 10c we present the distribution of the laminar lengths (waiting times) within the laminar region delimited by $\phi_0 = 0.000230$ and $\phi_L = 0.000329$, as well as, the corresponding fitting obtained using the fitting function $g(L)$ of Eq. (11), which implies that the specific distribution follows a power-law. Finally, Fig. 10d portrays the sets of the exponents p_2, p_3 of $g(L)$ obtained for different values of ϕ_L, from which one can verify that the MCF criticality conditions $p_2 > 1, p_3 \approx 0$ are satisfied for a wide region of ϕ_L values, implying a clear critical state.

Table 7 summarizes the criticality indications identified by the MCF analysis, for any of the seven studied VLF propagation paths, by providing details for the closest-in-time CW that was found in a time span of 15 days before each of the examined 2021 Thessaly EQs. In this table we include the date, the time of the detected CWs, the call name of the transmitter, the values of the exponents p_2 (maximum/mean) and p_3 (minimum/mean) and the possibly associated extreme event(s). We have found CWs in only five of the studied subionospheric propagation paths, while for the rest two (DHO-UWA and NRK-UWA) it was not possible to find a stationary nighttime time series excerpt, which it is a prerequisite for the MCF to be reliably applied. It is also mentioned that, although Table 7 includes only the closest-in-time CWs, more than one CWs were identified for the specific five paths prior to the 2021 Thessaly EQs which are attributed to them.

Finally, it is mentioned that for the FTA-UWA path we only found CWs before 1st 2021 Thessaly EQ but not before the 2nd 2021 Thessaly EQ, i.e., within the time period after the occurrence of the 1st and before the occurrence of the 2nd 2021 Thessaly EQ, while for the JXN-UWA and HWU-UWA paths, the transmitters were off for long time during the time period 2 March 2021 to 8 and 9 March 2021, respectively, and for this reason it was not possible to identify any CW related to the 2nd 2021 Thessaly EQ in these two paths.

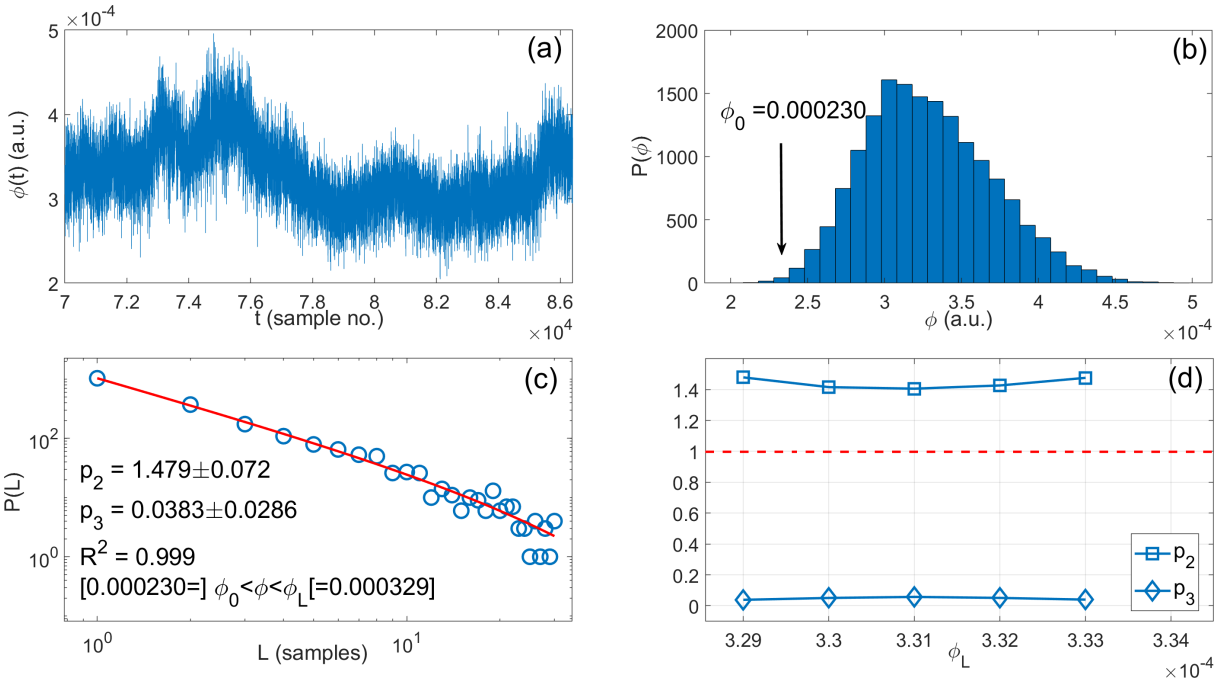

Figure 10. MCF analysis of the VLF time series excerpt from 70,000 s to 86,400 s of the ICV-UWA propagation path recordings of 02 March 2021, ~1 day prior to the 1st 2021 Thessaly EQ. (a) The analyzed time series excerpt, where time is expressed as the sample number within the specific day (sampling of a day starts at 00:00 UT, sampling rate = 1 Hz, i.e., 1 sps). (b) The amplitude distribution of the time series excerpt of Fig. 10a, from which $\phi_0 = 0.000230$ was determined. (c) The distribution of the laminar lengths and the corresponding fitting using Eq. (11) (red solid line) for the laminar region determined by $\phi_0 = 0.000230$ and $\phi_L = 0.000329$; $R^2 \approx 1$ indicates an excellent fit. (d) The estimated values of the exponents p_2, p_3 for different values of the end of the laminar region ϕ_L. The red dashed horizontal line indicates the critical limit ($p_2 = 1$); the MCF analysis criticality conditions $p_2 > 1$ and $p_3 \cong 0$ are satisfied for a wide range of ϕ_L values.

Transmitter	Date (UT)	Analyzed Time Window (UT)	$p_{2.max}/p_{2.mean}$	$p_{3.min}/p_{3.mean}$	Possibly Associated Extreme Event(s)
JXN	28 February 2021	00:00:00 – 04:26:39	1.443/1.375	0.0349/0.0493	a
GBZ	2 March 2021	01:40:00 – 03:20:00	1.691/1.615	0.0125/0.0248	a
	4 March 2021	01:06:40 – 02:30:00	1.498/1.306	0.0033/0.0268	b
ICV	2 March 2021	19:26:39 – 23:59:59	1.479/1.440	0.0383/0.0472	a
	4 March 2021	00:00:00 – 04:26:39	1.087/1.044	0.0246/0.0315	b
FTA	2 March 2021	01:39:59 – 04:26:39	1.438/1.414	0.0497/0.0561	a
HWU	27 February 2021	01:40:00 – 03:20:00	1.552/1.464	0.0125/0.0238	a
The following letters appearing in the column "Possible associated earthquakes with respect to the detected CW" denote, respectively: a→1st 2021 Thessaly EQ (6.3 M_w, 3 March 2021); b→2nd 2021 Thessaly EQ (5.8 M_w, 4 March 2021)					

Table 7. MCF analysis results. The revealed critical dynamics are denoted by the call name of the transmitter(s) of the path(s) for which MCF analysis criticality conditions were found to be satisfied.

5. Conclusions

This work elaborately presented the multi-method analysis of multiple paths' VLF subionospheric propagation data of an adequately long time period around (> 1 month before and ~15 days after) two strong EQs ($M_w = 6.3$ and $M_w = 5.8$) that hit north-central mainland Greece (Thessaly), at very close locations, with time difference of < 1 day, on 3 and 4 March of 2021, respectively. Specifically, the data acquired by the UWA VLF radio receiver, which is located in Athens (Greece), from seven VLF transmitters located north-northwest to the receiver have been used, on the grounds that the 2021 Thessaly EQs' epicenters were located within the corresponding paths' fifth Fresnel zones, or (in the case of the ICV-UWA path) close to its borders. The applied analysis identified statistical anomalies in the nighttime amplitude (revealed by the NFM method), statistical anomalies in the TTs (revealed by the TTM method), wave-like structures indicating AGW-related anomalies (revealed by the Morlet wavelet scalograms), as well as criticality signatures (revealed by the NT and MCF methods) in different dates and different sub ionospheric propagation paths (see Tables 3-7) within 15 days before the occurrence of the 2021 Thessaly EQs. Therefore, we conclude that there are multiple indications that the lower ionosphere was indeed disturbed due to the preparation processes of the above-mentioned EQs, offering different types of seismogenic indications in relation to the 2021 Thessaly EQs. Figure 11 summarizes all the types of anomalies and criticality signatures revealed for the 2021 Thessaly EQs.

It is finally mentioned that any possibly ionosphere-influencing extreme events (e.g., geomagnetic storms, EQs with $M_w \geq 5.5$ and volcanoes), other than the EQs under study, that occurred during the examined time period have been discussed in detail, whereas any possible attribution of the revealed anomalies and criticality signatures to them has been included in Tables 3-7. Since the analyzed time period was in general quiet in terms of space and weather phenomena, most of the indications found which were not attributed to the 2021 Thessaly EQs were attributed to other EQs that occurred along the studied propagation paths, except for those attributed to a volcano eruption. In general, all detected anomalies were possible to be explained in terms of possibly ionosphere-influencing phenomena, proving the ground-based lower ionosphere observation a valuable tool in studying ionosphere's perturbations due to any phenomena.

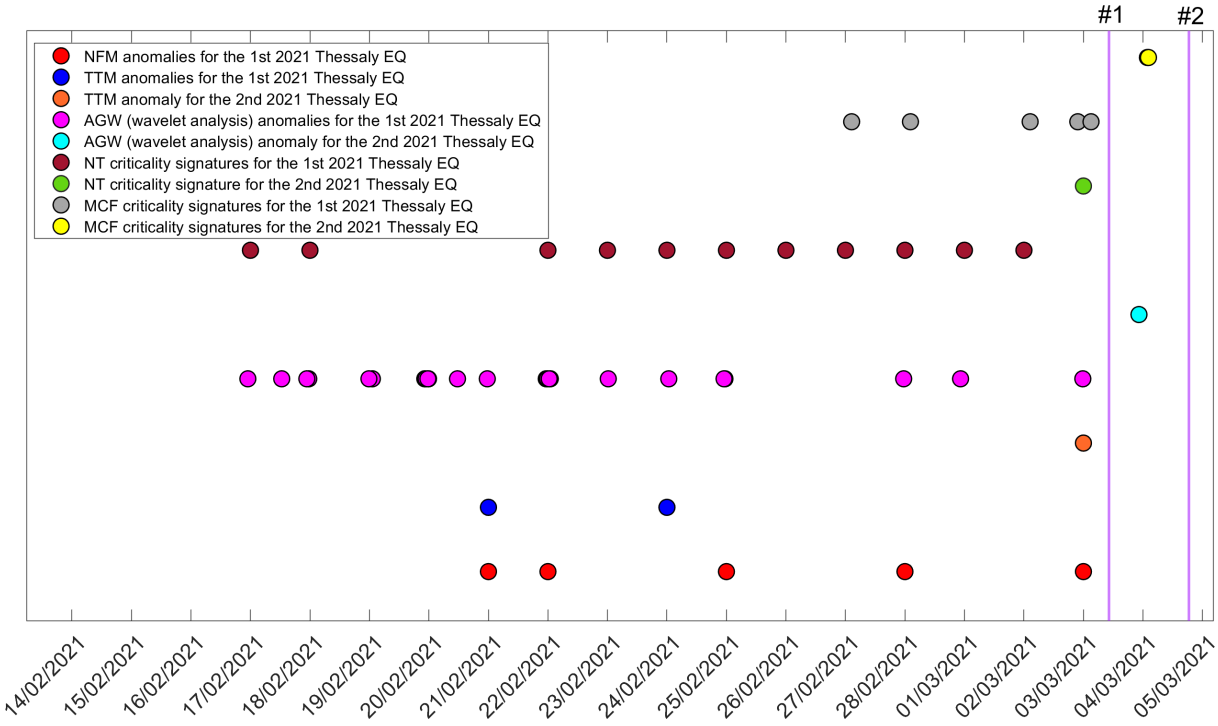

Figure 11. Timeline of all the detected anomalies and criticality signatures related with the 2021 Thessaly EQs as acquired from Tables 3-7. The colored (with different colors) circles indicate the type of anomaly or criticality signature. The two solid vertical purple lines illustrate the time of occurrence of the 2021 Thessaly EQs.

Acknowledgements. The authors would like to express their gratitude to the United States Geological Survey for the seismic catalog, to the World Data Center for Geomagnetism of Kyoto for the geomagnetic indices Dst, Kp, ap, and Ap data, to the USA National Oceanic and Atmospheric Administration for the solar X-ray flux data, to the Global Volcanism Program of the Smithsonian Institution for the volcano eruption data, to the Ventusky search engine, the USA National Oceanic and Atmospheric Administration (NOAA), and the DeutscherWetter-dienst (DWD) for the CAPE parameter data, as well as to Blitzortung.org and lightningmaps.org for the lightning activity data. The authors would also like to thank the anonymous reviewers for their comments that helped improving the manuscript. Finally, Mr. Politis would like to thank Mr. Sagardweep Biswas for his helpful discussions concerning the application of the wavelet analysis to VLF sub-ionospheric propagation data.

References

Abe, S., N.V. Sarlis, E.S. Skordas, H.K. Tanaka and P.A. Varotsos (2005). Origin of the usefulness of the natural-time representation of complex time series. Phys. Rev. Lett., 94, 170601. https://doi.org/10.1103/PhysRevLett.94.170601

Balasis, G., I.A. Daglis, Y. Contoyiannis, S.M. Potirakis, C. Papadimitriou, N.S. Melis, O. Giannakis, A. Papaioannou, A. Anastasiadis and C. Kontoes (2018). Observation of Intermittency-Induced critical dynamics in geomagnetic field time series prior to the intense magnetic storms of March, June, and December 2015, J. Geophys. Res. Space Phys., 123, 4594-4613. https://doi.org/10.1002/2017JA025131

Biswas, S., S. Kundu, S. Ghosh, S. Chowdhury, S.-S. Yang, M. Hayakawa, S. Chakraborty, S.K. Chakrabarti and S. Sasmal (2020). Contaminated effect of geomagnetic storms on pre-seismic atmospheric and ionospheric anomalies during Imphal earthquake, Open J. Earthq. Res, 09, 383-402, https://doi.org/10.4236/ojer.2020.95022

Biswas, S., S. Chowdhury, S. Sasmal, D.Z. Politis, S.M. Potirakis and M. Hayakawa (2022). Numerical modelling of sub-ionospheric very low frequency radio signal anomalies during the Samos (Greece) earthquake (M = 6.9) on October 30, 2020, Adv. Space Res., 70, 5, 1453-1471, https://doi.org/10.1016/j.asr.2022.06.016

Chakrabarti, S.K., M. Saha, R. Khan, S. Mandal, K. Acharyya and R. Saha (2005). Possible detection of ionospheric disturbances during the Sumatra-Andaman islands earthquakes of December, 2004, Indian J. Radio Sp. Phys., 34, 314-317, http://nopr.niscpr.res.in/handle/123456789/25665

Chakrabarti, S., S. Sasmal, M. Saha, R. Khan, D. Bhoumik and S.K. Chakrabarti (2007). Unusual behavior of D-region ionization time at 18.2kHz during seismically active days, Indian J. Phys., 81, 5, 531-538.

Chakrabarti, S.K., S. Sasmal and S. Chakrabarti (2010). Ionospheric anomaly due to seismic activities—Part 2: Evidence from D-Layer preparation and disappearance times, Nat. Haz. Earth Syst. Sci., 10, 1751-1757, https://doi.org/10.5194/nhess-10-1751-2010

Chakraborty, S., S. Sasmal, T. Basak, S. Ghosh, S. Palit, S.K. Chakrabarti and S. Ray (2017). Numerical modeling of possible lower ionospheric anomalies associated with Nepal earthquake in May, 2015, Adv. Space Res., 60, 8, 1787-1796, https://doi.org/10.1016/j.asr.2017.06.031

Chakraborty, S., S. Sasmal, S.K. Chakrabarti and A. Bhattacharya (2018). Observational signatures of unusual outgoing longwave radiation (OLR) and Atmospheric Gravity Waves (AGW) as precursory effects of May 2015 Nepal earthquakes, J. Geodyn., 113, 43-51, https://doi.org/10.1016/j.jog.2017.11.009

Christopoulos, S.-R.G., P.K. Varotsos, J. Perez-Oregon, K.A. Papadopoulou, E.S. Skordas and N.V. Sarlis (2022). Natural Time Analysis of Global Seismicity, Appl. Sci., 12, 7496, https://doi.org/10.3390/app12157496

Conti, L., P. Picozza and A. Sotgiu (2021). A critical review of ground based observations of earthquake precursors, Front. Earth Sci., 9, https://doi.org/10.3389/feart.2021.676766

Contoyiannis, Y. and F. Diakonos (2000). Criticality and intermittency in the order parameter space, Phys. Lett. A., 268, 286-292, https://doi.org/10.1016/S0375-9601(00)00180-8

Contoyiannis, Y.F., F.K. Diakonos and A. Malakis (2002). Intermittent dynamics of critical fluctuations, Phys. Rev. Lett., 89, 035701, https://doi.org/10.1103/PhysRevLett.89.035701

Contoyiannis, Y.F., F. Diakonos, P. Kapiris, A. Peratzakis and K. Eftaxias (2004a). Intermittent dynamics of critical pre-seismic electromagnetic fluctuations, Phys. Chem. Earth Parts A/B/C, 29, 397-408, https://doi.org/10.1016/j.pce.2003.11.012

Contoyiannis, Y.F., F.K. Diakonos, C. Papaefthimiou and G. Theophilidis (2004b). Criticality in the relaxation phase of a spontaneously contracting atria isolated from a frog's heart, Phys. Rev. Lett., 93, 098101, https://doi.org/0.1103/PhysRevLett.93.098101

Contoyiannis, Y.F. and F.K. Diakonos (2007). Unimodal maps and order parameter fluctuations in the critical region. Phys. Rev. E., 76, 031138, https://doi.org/10.1103/PhysRevE.76.031138

Contoyiannis, Y.F., S.M. Potirakis and K. Eftaxias (2013). The Earth as a living planet: human-type diseases in the earthquake preparation process, Nat. Hazards Earth Syst. Sci., 13, 125-139, https://doi.org/10.5194/nhess-13-125-2013

Contoyiannis, Y. and S.M. Potirakis (2018). Signatures of the symmetry breaking phenomenon in pre-seismic electromagnetic emissions, J. Stat. Mech., 2018, 083208. https://doi.org/10.1088/1742-5468/aad6ba

Contoyiannis, Y., F.K. Diakonos, M. Kampitakis and S.M. Potirakis (2021). Can high-frequency ECG fluctuations differentiate between healthy and myocardial infarction cases, Adv. Biomed. Eng., 2, 100011, https://doi.org/10.1016/j.bea.2021.100011

Das, B., A. Sen, P.K. Haldar and S. Pal (2021). VLF radio signal anomaly associated with geomagnetic storm followed by an earthquake at a subtropical low latitude station in northeastern part of India, Indian J. Phys. Appl., 96, 1, 13-24, https://doi.org/10.1007/s12648-020-01966-2

Daubechies, I. (1992). Ten lectures on wavelets, Society for Industrial and Applied Mathematics, Philadelphia, https://doi.org/10.1137/1.9781611970104

Eftaxias, K., S.M. Potirakis and Y. Contoyiannis (2018). Four-stage model of earthquake generation in terms of fracture-induced electromagnetic emissions. Complexity of Seismic Time Series, 437-502, https://doi.org/10.1016/b978-0-12-813138-1.00013-4

Ghosh, S., S. Chakraborty, S. Sasmal, T. Basak, S.K. Chakrabarti and A. Samanta (2019). Comparative study of the possible lower ionospheric anomalies in very low frequency (VLF) signal during Honshu, 2011 and Nepal, 2015 earthquakes, Geomat. Nat. Hazards Risk, 10, 1596-1612, https://doi.org/10.1080/19475705.2019.1595178

Ghosh, S., S. Chowdhury, S. Kundu, S. Sasmal, D.Z. Politis, S.M. Potirakis, M. Hayakawa, S. Chakraborty and S.K. Chakrabarti (2021). Unusual surface latent heat flux variations and their critical dynamics revealed before strong earthquakes, Entropy, 24, 1, 23, https://doi.org/10.3390/e24010023

Ghosh, S., S. Sasmal, M. Naja, S. Potirakis and M. Hayakawa (2023). Study of aerosol anomaly associated with large earthquakes, Adv. Space Res., 71, 1, 129-143, https://doi.org/10.1016/j.asr.2022.08.051

Hayakawa, M., O.A. Molchanov, T. Ondoh and E. Kawai (1996a). The Precursory Signature Effect of the Kobe Earthquake on VLF Sub-Ionospheric Signals. J. Comm. Res. Lab., 43, 2, 169-180.

Hayakawa, M., O.A. Molchanov, T. Ondoh and E. Kawai (1996b). Anomalies in the sub-ionospheric VLF signals for the 1995 Hyogo-Ken Nanbu earthquake, J. Phys. Earth, 44, 4, 413-418, https://doi.org/10.4294/jpe1952.44.413

Hayakawa, M. (2007). VLF/LF Radio Sounding of Ionospheric Perturbations Associated with Earthquakes, Sensors, 7, 1141-1158, https://doi.org/10.3390/s7071141

Hayakawa, M. (2011). Probing the lower ionospheric perturbations associated with earthquakes by means of subionospheric VLF/LF propagation, Earthq. Sci., 24(6), 609-637. https://doi.org/10.1007/s11589-011-0823-1

Hayakawa, M. (2019). Seismo electromagnetics and earthquake prediction: History and new directions, Int. J. Elect. App. Res., 06, 01, 1-23, https://doi.org/10.33665/ijear.2019.v06i01.001

Hayakawa, M., J. Izutsu, A. Schekotov, S.-S. Yang, M. Solovieva and E. Budilova (2021). Lithosphere-atmosphere-ionosphere coupling effects based on multiparameter precursor observations for February-March 2021 earthquakes (M~7) in the offshore of Tohoku area of Japan, Geosciences, 11, 11, 481, https://doi.org/10.3390/geosciences11110481

Hayakawa, M., A. Schekotov, S. Izutsu, S.-S. Yang, M. Solovieva and Y. Hobara (2022). Multi-parameter observations of seismogenic phenomena related to the Tokyo earthquake (M = 5.9) on 7 October 2021, Geosciences, 12, 7, 265, https://doi.org/10.3390/geosciences12070265

Huang, K. (1987). Statistical mechanics, Wiley, New York.

Kawamura, H., T. Hatano, N. Kato, S. Biswas and B.K. Chakrabarti (2012). Statistical physics of fracture, friction, and earthquakes, Rev. Mod. Phys., 84, 2, 839-884, https://doi.org/10.1103/revmodphys.84.839

Kosmidis, E.K., Y.F. Contoyiannis, C. Papatheodoropoulos and F.K. Diakonos (2018) Traits of criticality in membrane potential fluctuations of pyramidal neurons in the CA 1 region of rat hippocampus, Eur. J. Neurosci., 2018, 48, 2343-2353, https://doi.org/10.1111/ejn.14117

Kumar, A. and S. Kumar (2014). Space weather effects on the low latitude D-region ionosphere during solar minimum, Earth, Planets and Space, 66, 1, https://doi.org/10.1186/1880-5981-66-76

Mallat, S. (1998). A wavelet tour of signal processing, Academic Press, https://doi.org/10.1016/b978-0-12-466606-1.x5000-4

Malkotsis, F., D.Z. Politis, D. Dimakos and S.M. Potirakis (2022). An amateur-radio-based open-source (HW/SW) VLF/LF receiver for lower ionosphere monitoring, examples of identified perturbations, Foundations, 2, 3, 639-663, https://doi.org/10.3390/foundations2030044

Maurya, A.K., K. Venkatesham, P. Tiwari, K. Vijaykumar, R. Singh, A.K. Singh and D.S. Ramesh (2016). The 25 April 2015 Nepal earthquake: Investigation of Precursor in VLF Subionospheric Signal, J. Geophys. Res. Space Phys., 121, 10, https://doi.org/10.1002/2016ja022721

Molchanov, O.A. and M. Hayakawa (1995). Generation of ULF electromagnetic emissions by microfracturing, Geophys. Res. Lett., 22, 22, 3091-3094, https://doi.org/10.1029/95GL00781

Molchanov, O.A., M. Hayakawa, T. Ondoh and E. Kawai (1998). Precursory effects in the sub-ionospheric VLF signals for the Kobe earthquake, Phys. Earth Planet. Inter., 105, 239-248, https://doi.org/10.1016/S0031-9201(97)00095-2

Molchanov, O.A. and M. Hayakawa (2008). Seismo-Electromagnetics and Related Phenomena: History and Latest Results, Terrapub, Tokyo.

Nina, A., P.F. Biagi, S.T. Mitrović, S. Pulinets, G. Nico, M. Radovanović and L.Č. Popović (2021). Reduction of the VLF signal phase noise before earthquakes, Atmosphere, 12, 4, 444, https://doi.org/10.3390/atmos12040444

Pal, P., S. Sasmal and S.K. Chakrabarti (2017). Studies of seismo-ionospheric correlations using anomalies in phase of very low frequency signal, Geomat. Nat. Haz. Risk, 8, 167-176, https://doi.org/10.1080/19475705.2016.1161666

Picozza, P., L. Conti and A. Sotgiu (2021). Looking for earthquake precursors from space: A critical review, Front. Earth Sci., 9, https://doi.org/10.3389/feart.2021.676775

Piersanti, M., M. Materassi, R. Battiston, V. Carbone, A. Cicone, G. D'Angelo, P. Diego and P. Ubertini (2020). Magnetospheric-ionospheric-lithospheric coupling model. 1: Observations during the 5 August 2018 Bayan earthquake, Remote Sens., 12, 20, 3299, https://doi.org/10.3390/rs12203299

Politis, D.Z., S.M. Potirakis, Y.F. Contoyiannis, S. Biswas, S. Sasmal and M. Hayakawa (2021). Statistical and criticality analysis of the lower ionosphere prior to the 30 October 2020 Samos (Greece) earthquake (M6.9), based on VLF electromagnetic propagation data as recorded by a new VLF/LF receiver installed in Athens (Greece), Entropy, 23, 6, 676, https://doi.org/10.3390/e23060676

Politis, D.Z., S.M. Potirakis, S. Kundu, S. Chowdhury, S. Sasmal and M. Hayakawa (2022). Critical dynamics in stratospheric potential energy variations prior to significant (M > 6.7) earthquakes, Symmetry, 14, 1939, https://doi.org/10.3390/sym14091939

Potirakis, S.M., A. Karadimitrakis and K. Eftaxias (2013). Natural time analysis of critical phenomena: The case of pre-fracture electromagnetic emissions, Chaos, 23, 2, 023117, https://doi.org/10.1063/1.4807908

Potirakis, S.M., K. Eftaxias, A. Schekotov, H. Yamaguchi and M. Hayakawa (2016). Criticality features in ultra-low frequency magnetic fields prior to the 2013 M6.3 Kobe earthquake, Annals of Geophysics, 59, 3, S0317, https://doi.org/10.4401/ag-6863

Potirakis, S.M., Y. Contoyiannis, F.K. Diakonos and M.P. Hanias (2017). Intermittency-induced criticality in a resistor-inductor-diode circuit, Phys. Rev. E, 95, 042206. https://doi.org/10.1103/PhysRevE.95.042206

Potirakis, S.M., T. Asano and M. Hayakawa (2018a). Criticality analysis of the lower ionosphere perturbations prior to the 2016 Kumamoto (Japan) earthquakes as based on VLF electromagnetic wave propagation data observed at multiple stations, Entropy, 20, 3, 199, https://doi.org/10.3390/e20030199

Potirakis, S.M., Y. Contoyiannis, T. Asano and M. Hayakawa (2018b). Intermittency-induced criticality in the lower ionosphere prior to the 2016 Kumamoto earthquakes as embedded in the VLF propagation data observed at multiple stations, Tectonophysics, 722, 422-431, https://doi.org/10.1016/j.tecto.2017.11.020

Potirakis, S.M., Y. Contoyiannis, A. Schekotov, T. Asano and M. Hayakawa (2019). Analysis of the ultra-low frequency magnetic field fluctuations prior to the 2016 Kumamoto (Japan) earthquakes in terms of the method of critical fluctuations, Phys. A: Stat. Mech. App., 514, 563-572, https://doi.org/10.1016/j.physa.2018.09.070

Potirakis, S.M., Y. Contoyiannis, A. Schekotov, K. Eftaxias and M. Hayakawa (2021). Evidence of critical dynamics in various electromagnetic precursors, Eur. Phys. J. Spec. Top., 230, 151-177, https://doi.org/10.1140/epjst/e2020-000249-x

Potirakis, S.M., Y. Contoyiannis, K. Eftaxias, N.S. Melis and C. Nomicos (2022). Post-spontaneous-symmetry-breaking power-laws after a very strong earthquake: Indication for the preparation of a new strong earthquake or not? Phys. A: Stat. Mech. Appl., 589, 126607, https://doi.org/10.1016/j.physa.2021.126607

Pulinets, S. and K. Boyarchuk (2004). Ionospheric Precursors of Earthquakes, Springer, Berlin, https://doi.org/10.1007/978-94-024-2172-9

Pulinets, S. and D. Ouzounov (2011). Lithosphere-Atmosphere-Ionosphere Coupling (LAIC) Model—An Unified Concept for Earthquake Precursors Validation. J. Asian Earth Sci., 41, 371-382, https://doi.org/10.1016/j.jseaes.2010.03.005

Pulinets, S., D. Ouzounov, A. Karelin and K. Boyarchuk (2022). Earthquake Precursors in the Atmosphere and Ionosphere: New Concepts, Springer, Netherlands.

Ray, S., S.K. Chakrabarti, S. Sasmal, A.K. Choudhury and S.K. Chakrabarti (2010). Correlations between the anomalous behaviour of the ionosphere and the seismic events for VTX-MALDA VLF propagation, AIP conf. proc., 1286, 298, https://doi.org/10.1063/1.3512887

Ray, S., S.K. Chakrabarti, S.K. Mondal and S. Sasmal (2011). Ionospheric anomaly due to seismic activities-III: Correlation between night time VLF amplitude fluctuations and effective magnitudes of earthquakes in indian sub-sontinent, Nat. Hazards Earth Syst. Sci., 11, 2699-2704, https://doi.org/10.5194/nhess-11-2699-2011

Ray, S., S.K. Chakrabarti and S. Sasmal (2012). Precursory effects in the nighttime VLF signal amplitude for the 18th January, 2011 Pakistan earthquake, Indian J. Phys., 86, 85-88, https://doi.org/10.1007/s12648-012-0014-5

Ray, S. and S.K. Chakrabarti (2013). A study of the behavior of the terminator time shifts using multiple VLF propagation paths during the Pakistan earthquake (M = 7.2) of 18 January 2011, Nat. Hazards Earth Syst. Sci., 13, 1501-1506, https://doi.org/10.5194/nhess-13-1501-2013

Rozhnoi, A., M. Solovieva, O.A. Molchanov and M. Hayakawa (2004). Middle latitude LF (40 kHz) phase variations associated with earthquakes for quiet and disturbed geomagnetic conditions, Phys. Chem. Earth. A/B/C, 29 (4-9), 589-598, https://doi.org/10.1016/j.pce.2003.08.061

Rozhnoi, A., M. Solovieva and M. Hayakawa (2013). VLF/LF signals method for searching of electromagnetic earthquake precursors, Earthquake prediction studies: seismo electromagnetics M Hayakawa (Editor), Tokyo, Japan, 31-48.

Rozhnoi, A., M. Hayakawa, M. Solovieva, Y. Hobara and V. Fedun (2014a). Ionospheric effects of the Mt. Kirishima volcanic eruption as seen from Subionospheric VLF Observations, J. Atmos. Sol. Terr. Phys., 107, 54-59, https://doi.org/10.1016/j.jastp.2013.10.014

Rozhnoi, A., M. Solovieva, B. Levin, M. Hayakawa and V. Fedun (2014b). Meteorological effects in the lower ionosphere as based on VLF/LF Signal Observations, Nat. Hazards Earth Syst. Sci., 14, 10, 2671-2679, https://doi.org/10.5194/nhess-14-2671-2014

Sarlis, N.V., E.S. Skordas, M.S. Lazaridou and P.A. Varotsos (2008). Investigation of seismicity after the initiation of a seismic electric signal activity until the mainshock, Proc. Jpn. Acad. Ser. B, 84, 331-343, https://doi.org/10.2183/pjab/84.331

Sarlis, N.V., E.S. Skordas and P.A. Varotsos (2011). Similarity of fluctuations in systems exhibiting self-organized criticality, Europhys. Lett., 96, 28006, https://doi.org/10.1209/0295-5075/96/28006

Sasmal, S. and S.K. Chakrabarti (2009). Ionosperic anomaly due to seismic activities—Part 1: Calibration of the VLF signal of VTX 18.2 kHz station from Kolkata and deviation during seismic events, Nat. Hazards Earth Syst. Sci., 9, 1403-1408, https://doi.org/10.5194/nhess-9-1403-2009

Sasmal, S., S.K. Chakrabarti and S. Chakrabarti (2010). Studies of the correlation between ionospheric anomalies and seismic activities in the Indian subcontinent, AIP Conf. Proc., 1286, 270, https://doi.org/10.1063/1.3512885

Sasmal, S., S.K. Chakrabarti and S. Ray (2014). Unusual behavior of very low frequency signal during the earthquake at Honshu/Japan on 11 March, 2011, Indian J. Phys, 88, 1013-1019, https://doi.org/10.1007/s12648-014-0520-8

Sasmal, S., S. Chowdhury, S. Kundu, D.Z. Politis, S.M. Potirakis, G. Balasis, M. Hayakawa and S.K. Chakrabarti (2021). Pre-seismic irregularities during the 2020 Samos (Greece) earthquake (M = 6.9) as investigated from multi-parameter approach by ground and space-based techniques, Atmosphere, 12, 8, 1059, https://doi.org/10.3390/atmos12081059

Schuster, H.G. (1995). Deterministic Chaos: An Introduction, Wiley-VCH Verlag, Weinheim.

Stark, H.-G. (2005). Wavelets and Signal Processing: An application-based introduction, Springer-Verlag Berlin, Heidelberg, https://doi.org/10.1007/3-540-27481-2

Tatsuta, K., Y. Hobara, S. Pal and M. Balikhin (2015). Sub-ionospheric VLF signal anomaly due to geomagnetic storms: A statistical study, Annales Geophysicae, 33, 1457-1467, https://doi.org/10.5194/angeo-33-1457-2015

Torrence, C. and G.P. Compo (1998). A practical guide to wavelet analysis, Bull. Am. Meteorol. Soc., 79, 1, 61-78, https://doi.org/10.1175/1520-0477(1998)079<0061:apgtwa>2.0.co;2

Varotsos, P.A., N.V. Sarlis and E.S. Skordas (2001). Spatio-temporal complexity aspects on the interrelation between seismic electric signals and seismicity, Pract. Athens Acad., 76, 294-321.

Varotsos, P.A., N.V. Sarlis and E.S. Skordas (2002). Long-range correlations in the electric signals that precede rupture. Phys. Rev. E, 66, 011902, https://doi.org/10.1103/PhysRevE.66.011902

Varotsos, P.A. (2005). The Physics of Seismic Electric Signals, Terrapub, Tokyo.

Varotsos, P.A., N.V. Sarlis, H.K. Tanaka and E.S. Skordas (2005). Similarity of fluctuations in correlated systems: The case of seismicity, Phys. Rev. E, 72, 041103, https://doi.org/10.1103/PhysRevE.72.041103

Varotsos, P.A., N.V. Sarlis, E.S. Skordas, H.K. Tanaka and M.S. Lazaridou (2006). Entropy of seismic electric signals: Analysis in the natural time under time reversal, Phys. Rev. E, 73, 031114, https://doi.org/10.1103/PhysRevE.73.031114

Varotsos, P.A., N.V. Sarlis and E.S. Skordas (2011). Natural Time Analysis: The new view of Time, Precursory Seismic Electric Signals, Earthquakes and other Complex Time Series, Springer, Berlin, https://doi.org/10.1007/978-3-642-16449-1

Yang, S.-S., S.M. Potirakis, S. Sasmal and M. Hayakawa (2020). Natural Time Analysis of global navigation satellite system surface deformation: The case of the 2016 Kumamoto earthquakes, Entropy, 22, 6, 674. https://doi.org/10.3390/e22060674

Yoshida, M., T. Yamauchi, T. Horie and M. Hayakawa (2008). On the generation mechanism of terminator times in sub-ionospheric VLF/LF propagation and its possible application to seismogenic effects, Nat. Hazards Earth Syst., 8, 129-134, https://doi.org/10.5194/nhess-8-129-2008

Zitis, P.I., Y. Contoyiannis and S.M. Potirakis (2022). Critical dynamics related to a recent bitcoin crash, Int. Rev. Financ. Anal., 84, 102368, https://doi.org/10.1016/j.irfa.2022.102368

Zhao, S., X. Shen, L. Liao, Z. Zhima, C. Zhou, Z. Wang, J. Cui, and H. Lu (2020). Investigation of precursors in VLF subionospheric signals related to strong earthquakes (M>7) in western China and possible explanations, Remote Sens., 12(21), 3563, https://doi.org/10.3390/rs12213563

***CORRESPONDING AUTHOR: Stelios M. POTIRAKIS**,
Department of Electrical and Electronics Engineering, Ancient Olive Grove Campus,
University of West Attica, Egaleo-Athens, 12244, Greece
and Institute for Astronomy, Astrophysics, Space Applications and Remote Sensing,
National Observatory of Athens, Metaxa and Vasileos Pavlou, Penteli-Athens, 15236, Greece
e-mail: spoti@uniwa.gr